AWARD NUMBER: W81XWH-19-1-0535

TITLE: Astroglia Pathobiology in the Neurodegenerative Sequelae of Repetitive Mild Traumatic Brain Injury

PRINCIPAL INVESTIGATOR: Dr. Fiona Crawford

CONTRACTING ORGANIZATION: The Roskamp Institute, Inc.
2040 Whitfield Avenue,
Sarasota, FL
34243-3922

REPORT DATE: November 2023

TYPE OF REPORT: Final

PREPARED FOR: U.S. Army Medical Research and Development Command
Fort Detrick, Maryland 21702-5012

REPORT DOCUMENTATION PAGE

Form Approved
OMB No. 0704-0188

1. REPORT DATE:	**2. REPORT TYPE:**	**3. DATES COVERED:**
NOVEMBER 2023	**FINAL REPORT**	**1AUG2019 - 31JUL2023**

4. TITLE AND SUBTITLE:

Astroglia Pathobiology in the Neurodegenerative Sequelae of Repetitive Mild Traumatic Brain Injury

5a. CONTRACT NUMBER
W81XWH-19-1-0535

5b. GRANT NUMBER

5c. PROGRAM ELEMENT NUMBER

6. AUTHOR(S)
Fiona Crawford, PhD – Main PI; Joseph Ojo, PhD – Co-PI; Lauren Horne – Grant Coordinator

E-Mail: fcrawford@roskampinstitute.org; jojo@roskampinstitute.org; lhorne@roskampinstitute.org; cgil@roskampinstitute.org.

5d. PROJECT NUMBER

5e. TASK NUMBER

5f. WORK UNIT NUMBER

7. PERFORMING ORGANIZATION NAME(S) AND ADDRESS(ES)
The Roskamp Institute, Inc., 2040 Whitfield Avenue Sarasota, FL 34243-3922

8. PERFORMING ORGANIZATION REPORT

9. SPONSORING / MONITORING AGENCY NAME(S) AND ADDRESS(ES)

U.S. Army Medical Research and Development Command
Fort Detrick, Maryland 21702-5012

10. SPONSOR/MONITOR'S ACRONYM(S)

11. SPONSOR/MONITOR'S REPORT NUMBER(S)

12. DISTRIBUTION / AVAILABILITY STATEMENT: Approved for Public Release; Distribution Unlimited

13. SUPPLEMENTARY NOTES: N/A

14. ABSTRACT

For many years TBI has been known to be a risk factor for later life neurodegenerative diseases, such as Alzheimer's Disease Related Dementias (ADRD), but the precise nature of how TBI leads to or precipitates these conditions (or different pathological substrates) is not understood. We have spent years developing and characterizing mouse models of r-mTBI that demonstrate lifelong behavioral and neuropathological features of human TBI and are thus relevant models in which to generate data that will translate to human patients. In our mouse model, we observe dramatic increases in reactive astrocyte cells, and these increases last for life. We thus hypothesized that repetitive mTBI induces significant and persistent changes to reactive astrocyte populations after injury and that these reactive astroglial responses are critical to TBI neurodegeneration and, in the context of other potentially pathogenic proteins such as tau, distinct ADRD proteinopathies can be triggered. Here we propose neuropathological analyses of human autopsy cases of TBI, ADRD, and from the brains of normal mice and mice producing potentially pathological tau proteins (in neurons vs astrocytes), at a range of timepoints following repetitive mild TBI. We have analyzed astrocyte lesions in tissue from our mouse models and observe qualitative and quantitative changes to astrocyte morphologies following injury. We explored the role of astrocytes in inducing and driving pathogenesis by utilizing novel mechanistic approaches in our mouse models, involving intracerebral injections of TBI/sham astroglial secretome into naïve mice, and utilizing *ex vivo* functional assays to closely study whether reactive astrocytes in the injured brain can activate ex vivo microglial inflammatory response(s). Finally, we used our state-of-the-art single cell genomic analyses to reveal astrocyte specific changes at the gene level in our mouse model that shared some overlap with changes in autopsy tissue analyzed by Laser Capture Microdissection (LCM) and gene array.

15. SUBJECT TERMS: TBI, ADRD, Astrocytes, Neuropathology, Transcriptomics, Single cell profiling, Animal models

16. SECURITY CLASSIFICATION OF:			**17. LIMITATION OF ABSTRACT**	**18. NUMBER OF PAGES**	**19a. NAME OF RESPONSIBLE PERSON**
					USAMRDC
a. REPORT	**b. ABSTRACT**	**c. THIS PAGE**			**19b. TELEPHONE NUMBER** *(include area code)*
U	U	U	UU	**50**	

Standard Form 298 (Rev. 8-98)
Prescribed by ANSI Std. Z39.18

TABLE OF CONTENTS

INTRODUCTION:

In this project we will interrogate the role of astrocytes in inducing and driving TBI related neurodegeneration by utilizing neuropathological tools to characterize astrocyte lesions in mouse models and autopsy tissue of TBI and ADRD cases. We will also use our novel mechanistic approaches involving adoptive cell transfer and *ex vivo* functional assays to clarify the means through which astrocytes contribute to TBI-neurodegeneration and precipitation of ADRD. We will conclude by applying our state-of-the-art single cell gene profiling to interrogate astrocytes from our mouse models and autopsy cases to identify astrocyte specific changes at the gene and protein level, and to identify novel single cell targets to interrupt the pathobiological consequences of TBI.

1. KEYWORDS:

TBI, ADRD, Astrocytes, Neuropathology, Transcriptomics, Single cell profiling, Animal models, Ex Vivo Models.

2. ACCOMPLISHMENTS:

The PI is reminded that the recipient organization is required to obtain prior written approval from the awarding agency grants official whenever there are significant changes in the project or its direction.

What were the major goals of the project?

List the major goals of the project as stated in the approved SOW. If the application listed milestones/target dates for important activities or phases of the project, identify these dates and show actual completion dates or the percentage of completion.

HYPOTHESIS

Repetitive mTBI induces significant and persistent changes to reactive astrocyte populations after injury. These reactive astroglial responses are critical to TBI neurodegeneration and, in the context of other potentially pathogenic proteins such as tau or amyloid, distinct ADRD proteinopathies can be triggered.

MAJOR TASK 1: (a) *Delineation of the chronic effects of repetitive mTBI on astrogliopathy and related proteinopathy in wild type and humanized tau mouse models at 3 months and 6 months post-injury****. (1b)*** *Investigation of astroglial pathological lesions in autopsied brains from human TBI, age-related tau astrogliopathy (ARTAG), and ADRD cases.*
MAJOR TASK 2: *Evaluating pathobiological effects of reactive/injured astrocytes derived from mouse models in Aim 1, on the induction and spreading of age-related proteinopathies and neurodegeneration.*
MAJOR TASK 3: (a) *Generation of single cell genomic/secretome profiles in astrocyte populations obtained from mouse models described in Aim 1.* ***(b)*** *Single cell genomic profiling of astrocyte populations in autopsied brains from TBI and ADRD cases.*

PROJECT MILESTONES/DELIVERABLES

1: Detailed timeline and dynamics of astroglia lesions (using histopathology) in response to injury, ageing, and proteinopathies in animal models, and correlation with neuropathological staging in human r-mTBI/ADRD autopsy cases. [Month 1-27]

2: To determine whether reactive astrocytes from the injured brain milieu of our TBI models are sufficient to induce and drive age-related proteinopathies and neurodegeneration. [Month 7-32]

3: Novel gene and secreted protein expression profiles of astroglia populations in TBI mediated neurodegeneration, normal ageing and ADRD pathogenesis in mouse models and autopsy cases. [Month 7-36]

What was accomplished under these goals?

For this reporting period describe: 1) major activities; 2) specific objectives; 3) significant results or key outcomes, including major findings, developments, or conclusions (both positive and negative); and/or 4) other achievements. Include a discussion of stated goals not met. Description shall include pertinent data and graphs in sufficient detail to explain any significant results achieved. A succinct description of the methodology used shall be provided. As the project progresses to completion, the emphasis in reporting in this section should shift from reporting activities to reporting accomplishments.

Summary of accomplishments for each Aim.

MAJOR TASK 1:

(a) *Delineated the chronic effects of repetitive mTBI on astrogliopathy and related proteinopathy in young and aged wild type and humanized tau mouse models at 3 months and 6 months post-injury****. (b)*** *Investigated astroglial pathological lesions in autopsied brains from human TBI, age-related tau astrogliopathy (ARTAG), and ADRD cases****.***

MAJOR TASK 2: *Evaluated pathobiological effects of reactive/injured astrocytes derived from mouse models in Aim 1, on the induction and spreading of age-related proteinopathies and neurodegeneration.*

MAJOR TASK 3:

(a) *Generated single cell genomic/secretome profiles in astrocyte populations obtained from mouse models described in Aim 1.*

(b) *Generated Single cell genomic profiles of astrocytes in autopsied brains from TBI, ARTAG, ADRD cases.*

SUBTASK DESCRIPTIONS FOR MAJOR TASK 1

	Timeline	
Major Task 1	Months	
Subtask 1: Obtaining ACURO approval (Roskamp Institute approval for TBI procedures is already in place) and Human Cadaver use approval.	1-3	
Subtask 2: Breeding of cohorts for studies	1-6	
Substask 2a: Breeding of cohorts for Aged mice TBI studies (36 mice per genotype) at 3 & 6 months post-TBI	3-6	
Subtask 2b: Breeding of cohorts for Young mice TBI studies (36 mice per genotype)	3-6	
Subtask 3: Histopathological analyses of astroglia lesions in autopsy cases. N=10/group; 100 samples. Samples are coded and de-identified.	1-9	
Subtask 4: Administering injuries to Young cohort - 3 months old at injury. For each of the genotypes there will be two groups - 18 r-mTBI young and 18 r-sham young.	6-9	
Subtask 5: Euthanasia of Young cohort in subtask 4.	6-16	
Subtask 6: Sectioning and histopathological staining of Young cohort tissues with astroglia, tau and synaptic antibodies.	13-18	
Subtask 7: Stereological analyses and Image quantitation of brain sections from Young cohort (staggered over time)	13-21	
Subtask 8: Administering injuries to Aged cohort (i.e. 12 months old at injury). Animals will receive injuries as in subtask 4.	15-18	
Subtask 9: Euthanasia of Aged cohort in subtask 8	15-25	
Subtask 10: Sectioning and histopathological staining of Aged cohort tissues with astroglia, tau and synaptic antibodies.	19-24	
Subtask 11: Stereological analyses and Image quantitation of brain sections from Aged cohort (staggered over time)	19-27	
Subtask 12: Interpretation of data/consultation with clinical neuropathologists	18-27	
Major Task 2		
Subtask 1: Breeding of cohorts for Young Donor mice for TBI studies in Subtask 2 and 3 (12 mice per genotype)	7-9	
Subtask 2: Administering injuries to Young ‘Donor’ cohort - 3 months old injury. Animals will receive injuries as in Major task 1 (subtask 4). For each of the genotypes there will be 6 r-mTBI and 6 r-sham .	9-12	
Subtask 3: Euthanasia of Young ‘Donor’ cohort from Subtask 1 at 10 months of age, isolation of astrocytes by magnetic cell sorting and injection into naïve ‘Recipient’ non-transgenic mouse brain. [Only secretome was injected]	21-24	
Subtask 4: Ex vivo experiment to determine pathobiological effects of exposing conditioned media derived from adult astrocyte cultures obtained from our transgenic TBI models, and their impact on healthy microglial cell lines.	21-27	

Subtask 5: Euthanasia of inoculated 'Recipient' naïve non-transgenic mice, collection of brain tissue, sectioning and histopathological staining with astroglia, tau and synaptic antibodies.	24-27	
Subtask 6: Stereological analyses and Image quantitation of brain sections from inoculated 'Recipient' cohort (staggered over time). Interpretation of data and consultation with clinical neuropathologists	28-32	
Major Task 3		
Subtask 1: Laser capture microdissection of astroglia from autopsy cases for single cell array for gene expression profiling. Same 10 groups and tissue sections from Major task 1 (subtask 3). N=8 cases/group; 80 samples.	7-15	
Subtask 2a: RNAseq of astroglia from Young Cohort (Major Task 1 – subtask 4) (staggered overtime). There will be 36 mouse brains per genotype for analyses.	15-24	
Subtask 2b: LC-MS/MS analyses of astroglia secretome from Young Cohort (Major Task 1 – subtask 4) mice for unbiased proteomic expression profiling (staggered overtime). There will be 36 astrocyte supernatants/ secretome collected from each mouse brain per genotype for analyses.	15-24	
Subtask 3a: RNAseq of astroglia from Aged Cohort (Major Task 1 – subtask 8) (staggered overtime). There will be 36 mouse brains per genotypes for analyses.	25-33	
Subtask 3b: LC-MS/MS analyses of astroglia secretome from Aged Cohort (Major Task 1 – subtask 8) for unbiased proteomic expression profiling.	25-33	
Subtask 4: Validation of select gene transcript profiles altered in astroglia (and protein profiles in the secretome), in both Young/Aged cohorts. rt-PCR, in situ hybridization, IHC, ELISA, etc.	21-33	
Subtask 5: Data analysis and interpretation and correlation studies	34-36	

AIM 1 - Part One: *Delineation of the chronic effects of repetitive mTBI on astrogliopathy and related proteinopathy in wild type and humanized tau mouse models at 3 months and 6 months post-injury.*

METHODOLOGY

Immunostaining: Briefly, sections were deparaffinized in xylene and rehydrated in a decreasing gradient of ethanol before the IHC procedure. Sections were rinsed in distilled water and subsequently incubated at room temperature in a solution of endogenous peroxidase blocking solution containing 3% hydrogen peroxide diluted in PBS for 15 minutes. For primary antibodies requiring antigen retrieval, sections were treated with either (I) DAKO target retrieval citrate buffer solution (pH 6) (Dako) for 8 minutes in the microwave, or (II) Tris-ethylene-diamine-tetra acetic acid—Tris-EDTA buffer (pH 8). Following antigen retrieval, sections were blocked for 1 hour in Dako protein serum-free protein block (Dako). Sections were immunostained in batches with primary antibodies made up in supersensitive wash buffer and antibody diluent background-reducing agent. After overnight incubation, sections were rinsed with PBS and transferred to a solution containing the appropriate conjugated (peroxidase or immunofluorescent) secondary antibody (Vectastain Elite ABC Kit, Vector Laboratories) for 1 hour, depending on the specific requirement of the antibody protocol. Immunoreactivity was visualized with a compatible chromogen or fluorophore attached to the secondary antibody. Development with the chromogen was timed and applied as a constant across batches to limit technical variability before progressing to quantitative image analysis. For DAB sections, mounted sections were progress through a graded series of alcohols (dehydrated), cleared in xylene, and cover-slipped with permanent mounting medium. For immunofluorescent antibodies, sections were mounted in fluorescent mounting medium. Immunoreacted DAB sections were viewed using a motorized Olympus (BX63) upright microscope and photographs taken using the high-resolution DP72 color digital camera. Immunofluorescent images were taken using a Zeiss LSM 800 confocal microscope. **Image Analysis:** Rigorous staining protocols were applied to ensure consistency of staining and accuracy of image analysis. Immunoreactivity for cell markers were measured by quantitative image analysis performed blind by investigator. Multiple ROI's were analyzed in standardized fashion for each marker. A survey of immunostained tissue sections was performed independently to verify specific immunoreactivity that will be subsequently used for quantitative image analysis. For immuno-DAB sections, non-overlapping red, green, blue (RGB) images were digitally captured randomly within the defined areas from each section, providing a systematic survey of each region of interest for each animal within a group. For immunofluorescent staining, images were captured using the Zeiss imaging software.

Briefly, a minimum of 20-30 microscopic fields (x20 or ×40 magnification) were analyzed per region. Immunoreacted profiles were optically segmented and analyzed using CellSens morphometric image analysis software (Olympus, Center Valley, Pennsylvania). A semi-automated RGB histogram-based protocol (specified in the image analysis program) was used to determine the optimal segmentation (threshold setting) for immunoreactivity for each antibody. Immunoreactive profiles discriminated in this manner were used to determine the specific immunoreactive percentage area estimates. **Western Blotting:** This was conducted using a standardized protocol (Ojo et al., 2018). Statistical analysis: All data presented, except bioinformatic data, was performed using GraphPad Prism Version 8. Data were tested for normality using the Shaphiro-Wilk test, if data were not normally distributed, data log transformation was applied. Then statistical analysis was obtained using Two-way ANOVA. When data remained with a non-normal distribution, non-parametric tests were performed. Data are presented as mean ±SEM. P values <0.05 were considered statistically significant. Graphs in the Results Section show asterisks representing different p-value ranges: < 0.05*; <0.01** and <0.001***.

MAJOR TASK 1 (Sub task – 11)

Astroglia and microglial reactivity at 3 & 6 months post-injury in WT, GFAP^{P301L} & CAMK2A^{P301L} mice

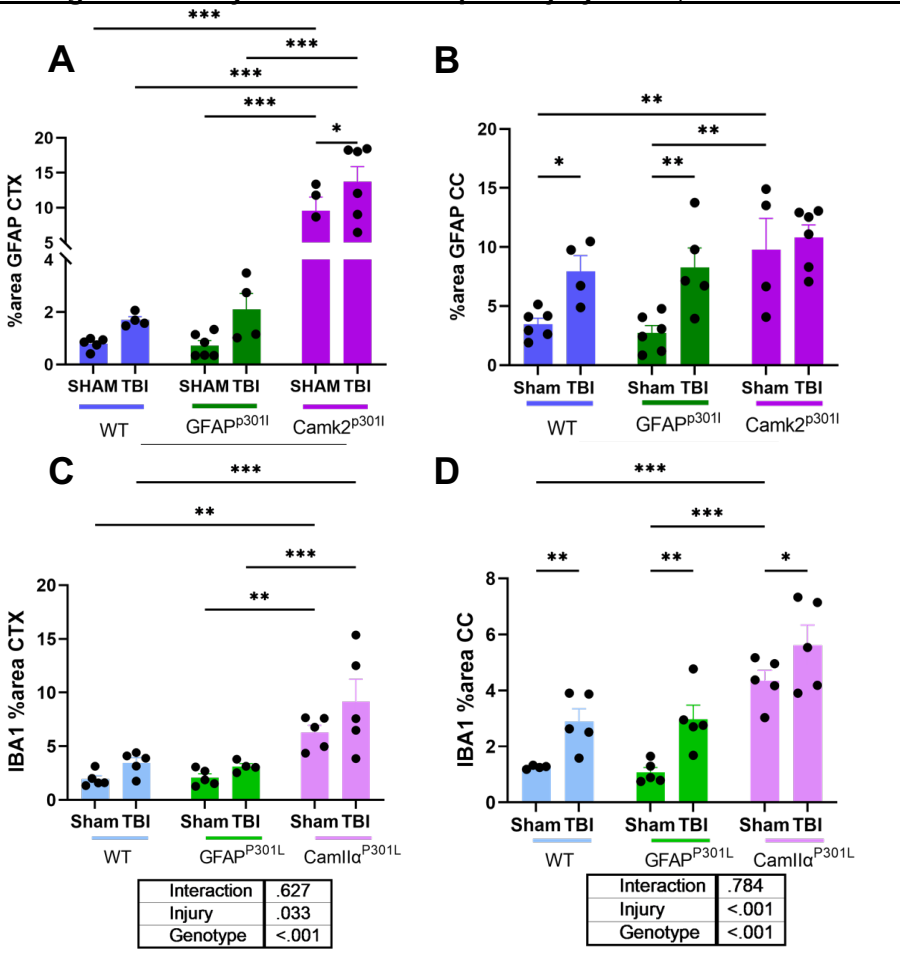

Figure 1. Quantification of reactive astrogliosis (GFAP) and microgliosis (IBA1) in the cortex (CTX) and corpus callosum (CC) of young WT, GFAP^{P301L} and CamK2A^{P301L} mice 3-months after r-mTBI. Percentage area of GFAP (A,B) and IBA1 (C,D). Data analyzed by Two-Way ANOVA. Asterisks denote: *P<0.05; **P<0.01 and ***P<0.001 for post-hoc analyses.

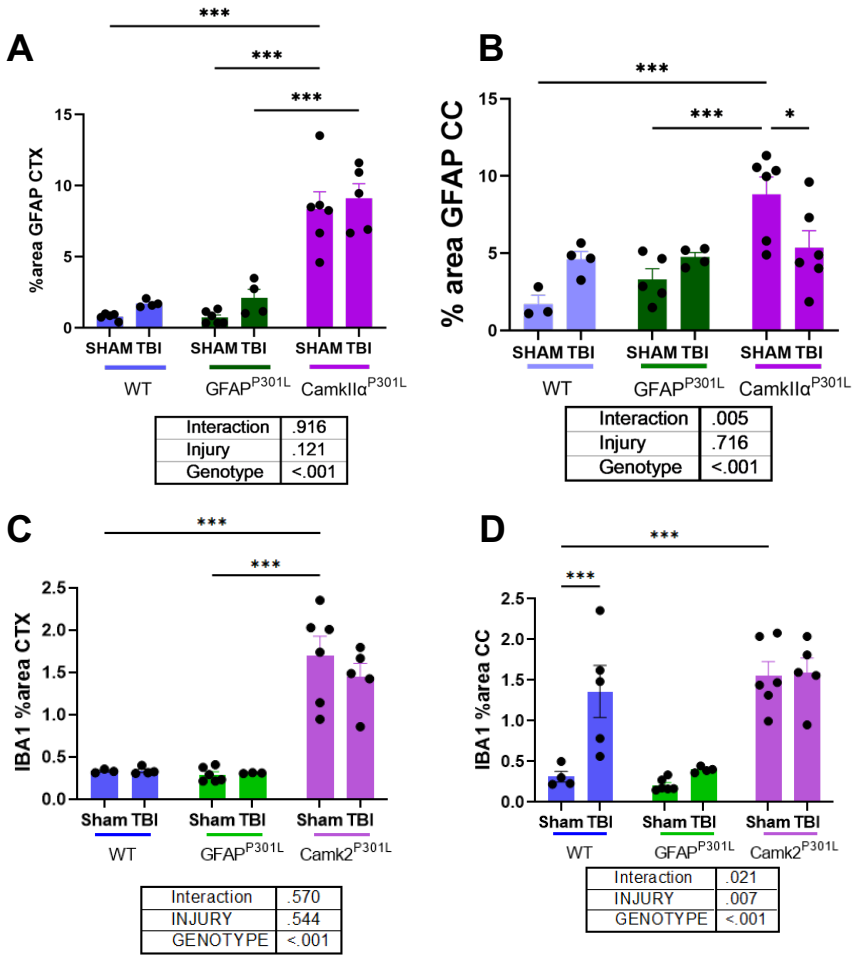

Figure 2. Quantification of reactive astrogliosis (GFAP) and microgliosis (IBA1) in the cortex (CTX) and corpus callosum (CC) of young WT, GFAP^{P301L} and CamK2A^{P301L} mice 6-months after r-mTBI. Percentage area of GFAP (A,B) and IBA1 (C,D). Data analyzed by Two-Way ANOVA. Asterisks denote: *P<0.05; **P<0.01 and ***P<0.001 for post-hoc analyses.

Summary

Genotype effects

To investigate the effect of astrocyte-derived and neuronal-derived tau on astrocyte and microglial morphological phenotype at baseline, we quantified the percentage area of GFAP and IBA1 immunoreactivity in the cortex and the *corpus callosum* (CC) to evaluate astrogliosis and microgliosis, respectively.

At 7mo of age, the presence of tau within astrocytes in the GFAP^{P301L} is not sufficient to elicit greater GFAP or IBA1 immunoreactivity in the cortex or CC (**Fig. 1A, B**) compared to WT. However, the presence of neuronal tau in the CamkIIα^{P301L} mice leads to a 10fold and a 3-fold increase in GFAP immunoreactivity within the cortex and CC, respectively, compared to both WT and GFAP^{P301L} (Fig. 2.1A&C). Additionally, IBA1 immunoreactivity in the cortex and CC of the CamkIIα^{P301L} is significantly greater compared to the other two genotypes. Those changes are represented by a 2-fold and 4-fold increase in the cortex and CC respectively (**Fig. 1 C, D**).

At 10 mo of age, there were no changes in GFAP and IBA1 immunoreactivity between WT and GFAP^{P301L} mice, while both markers were increased in the CamkIIα^{P301L} cohort in the cortex and CC (Fig. 2A-D). In the cortex of CamkIIα^{P301L} mice, we observed an 8-fold increase in GFAP immunoreactivity and a 4.5-fold increase in IBA1 immunoreactivity compared to WT and GFAP^{P301L}. In the CC of CamkIIα^{P301L} mice, there was a 4-fold increase in the IBA1 immunoreactivity compared to WT and GFAP^{P301L}.

Injury effects in the 3 genotypes

To investigate whether astroglial tau promotes exacerbated chronic neuroinflammatory outcomes three and six months after r-mTBI, we analyzed astrogliosis and microgliosis in the cortex and hippocampus of our three mouse models at three and six most post-last injury.

Three months post-last injury, there was a significant 1.5-fold increase in astrogliosis in the cortex of the CamkIIα^{P301L} r-mTBI group compared to their sham controls (**Fig. 1A**). Because astrogliosis in the CamkIIα^{P301L} model (both r-sham and r-mTBI mice cohorts) were disproportionately exacerbated compared to the other models, we therefore performed a separate Two-Way analyses using r-mTBI/sham WT and GFAP^{P301L} data only. Our analyses revealed that r-mTBI induced a significant 2-fold increase in GFAP immunoreactivity in both WT and GFAP^{P301L} cohorts when compared to their sham counterparts (**not shown**). Moreover, unlike exposure to exogenous tau (i.e., CamkIIα^{P301L} model), the presence of tau inside astrocytes (i.e., GFAP^{P301L} model) was not sufficient to evoke a worsened TBI response compared to WT counterparts. In the corpus callosum (CC), astrogliosis in WT and GFAP^{P301L} cohorts was increased 3 months post-last injury in the r-mTBI group compared to shams. In the case of the CamkIIα^{P301L} cohort, there is no TBI effect on astrogliosis in the CC (**Fig. 1B**). Furthermore, no augmented TBI effect was noted in the GFAP^{P301L} cohort compared to WT counterparts.

IBA1 immunoreactivity in the cortices of our mouse models demonstrated no significant changes in microgliosis in the CamkIIα^{P301L} cohort in the TBI group compared to the shams (**Fig. 1C**). As mentioned above, we also excluded the CamkIIα^{P301L} cohort data due to the disproportionate levels in IBA1 immunoreactivity between CamkIIα^{P301L} cohort and other genotypes, and ran our Two-Way statistical analysis on only the GFAP^{P301L} and WT groups. This analysis revealed that microgliosis is significantly increased in the TBI groups of both models compared to their sham counterparts (**not shown**). Additionally, the effect of r-mTBI exposure is not worsened in mice harboring tau-bearing astrocytes (GFAP^{P301L} cohort) compared to WT. In the CC of all cohorts, microgliosis is significantly increased in the TBI groups compared to the shams (**Fig. 1D**). Moreover, there is no difference in the TBI response in the GFAP^{P301L} cohort compared to the WT.

Six months post-last injury, no TBI effect on astrogliosis is observed across genotypes in the cortex (**Fig. 2A**) unless CamkIIα^{P301L} data is excluded from the Two Way ANOVA. Then, a significant 1.5-fold increase is observed in the r-mTBI group of both WT and GFAP^{P301L} compared to their respective sham counterparts (**Fig 2A; not shown**). In the CC, a significant TBI effect was observed in the CamkIIα^{P301L} cohort when all three genotypes were included in the Two Way ANOVA (**Fig. 2B**). When WT and GFAP^{P301L} cohorts were analyzed separately, we observed a significant injury effect in only the WT cohort (**Fig 2B; not shown**)

At six months post-last injury, there are no TBI-mediated changes in microgliosis across the cohorts within the cortex (**Fig. 2C**). In the CC, the TBI effect is persistent in the WT cohort represented by a 5-fold increase in the r-mTBI group compared to the r-sham. In the GFAP^{P301L} and CamkIIα^{P301L} cohort, there is no TBI effect on microgliosis (**Fig. 2D**). Moreover, there is no synergistic effect of TBI and tau within astrocytes on astrogliosis and microgliosis in the cortex or CC.

Altogether these data suggest that, unlike the presence of neuronal tau, the presence of pathological tau within astrocytes does not exacerbate the chronic reactive gliosis to r-mTBI at three and six months post-last injury.

Astroglia homeostatic markers at 3 & 6 mos post-injury in WT, GFAP^{P301L} and CAMK2A^{P301L} mice

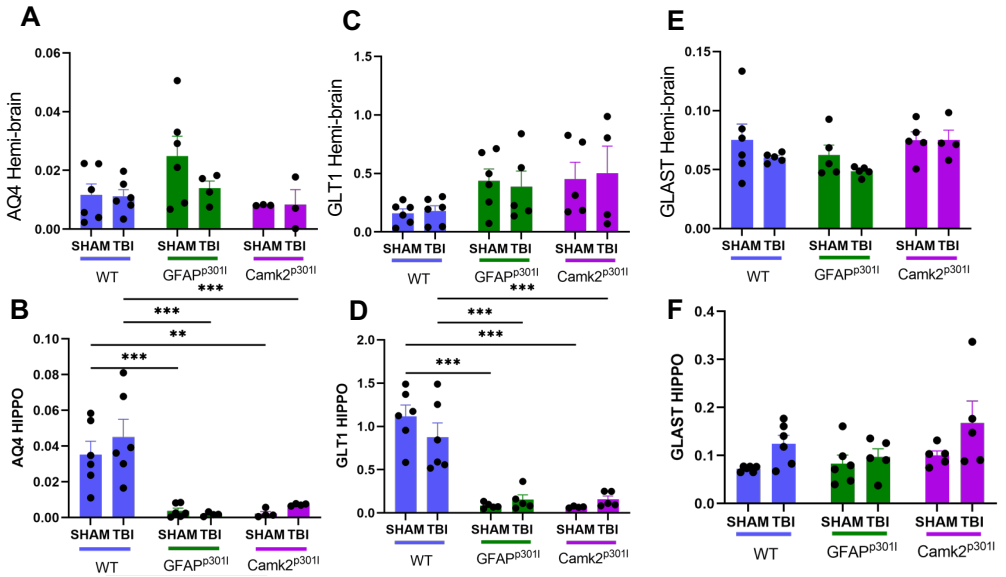

FIGURE 3. Changes in astrocyte homeostatic proteins in WT, GFAP^{P301L} and Camk2^{P301L} mice at 3 months post-injury. Levels of aquaporin 4 (AQ4) in the hemi-brain (**A**) and hippocampus (HIPPO, **B**); levels of glutamate transporters GLT1 and GLAST in the in the hemibrain and hippocampus (**C-F**) at 3 months post-last injury. Data analyzed by Two-Way ANOVA. Asterisks denote: *P<0.05; **P<0.01 and ***P<0.001 for post-hoc analyses.

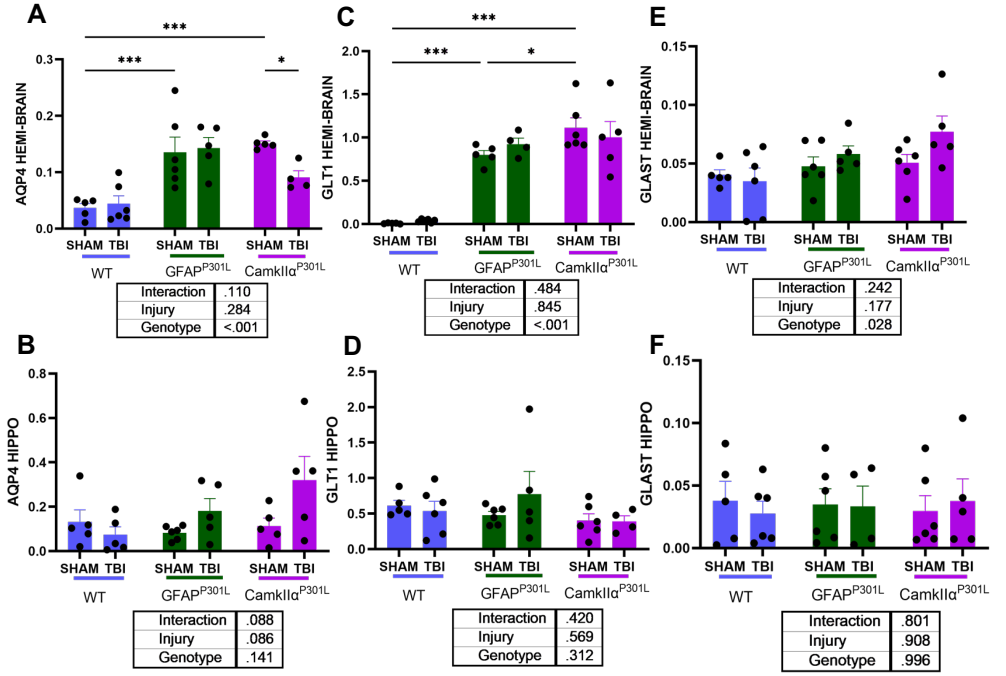

FIGURE 4. Changes in astrocyte homeostatic proteins in WT, GFAP^{P301L} and Camk2^{P301L} mice at 6 months post-injury. Levels of aquaporin 4 (AQ4) in the hemi-brain (**A**) and hippocampus (HIPPO, **B**); levels of glutamate transporters GLT1 and GLAST in the in the hemibrain and hippocampus (**C-F**) at 6 months post-last injury. Data analyzed by Two-Way ANOVA. Asterisks denote: *P<0.05; **P<0.01 and ***P<0.001 for post-hoc analyses.

Summary

Genotype effects

To investigate the influence of astroglial and neuronal tau on markers of astrocyte homeostasis, we assessed the protein levels of three common homeostatic markers by immunoblotting – the water channel aquaporin4 (AQ4) and the glutamate transporters (GLT1 and GLAST) – in the hemi-brain (i.e., *hemisphere minus hippocampus*) and hippocampus of our mouse models.

At 7 mo of age, no changes in the presence of AQ4, GLAST, and GLT1 are observed in the hemi-brain across the mouse models (**Fig. 3A,C,E**). However, a significant reduction in AQ4 and GLT1 protein levels is observed in the hippocampus of both tau models (GFAP^{P301L} and CamkIIα^{P301L}) compared to the WT (Fig. 3B,D). GLAST levels in the hippocampus remained unchanged across genotypes (Fig. 3F).

At 10 mo of age, there was a genotype effect in AQP4 and GLT1 levels in the hemi-brain, typified by an increase in GFAP^{P301L} and CamkIIα^{P301L} cohort's vs WT cohort (**Fig. 4A, C)**. Although a genotype effect by Two-way ANOVA was observed in GLAST levels in the hemi-brain, this was not significant by post-hoc analyses **(Fig 4E).** Paradoxically**,** no genotype effect by Two-way ANOVA was observed in AQP4, GLT1 or GLAST in the hippocampus **(Fig 4B,D,F).**

Injury effects in the 3 genotypes

To investigate the influence of tau astrogliopathy on astrocyte homeostasis after r-mTBI, we assessed the protein levels AQ4, GLT1, and GLAST in the hemi-brain and hippocampus of our mouse models.

At 3 mos post-last injury, the biochemical analysis reveals the absence of TBI-dependent changes in the levels of AQ4, GLT1, and GLAST in both regions of interest across the three genotypes (**Fig. 3A-F**).

At 6 mos post-last injury, the biochemical analysis revealed no TBI-dependent changes by Two-Way ANOVA in the levels of AQ4, GLT1, and GLAST in both regions of interest across the three genotypes (**Fig. 4A-F**). However, a notable reduction was observed in AQP4 in the hemibrain region (**Fig. 4A**).

Tau pathology at 3 and 6 months post-injury in WT, GFAP^{P301L} and CAMK2A^{P301L} mice

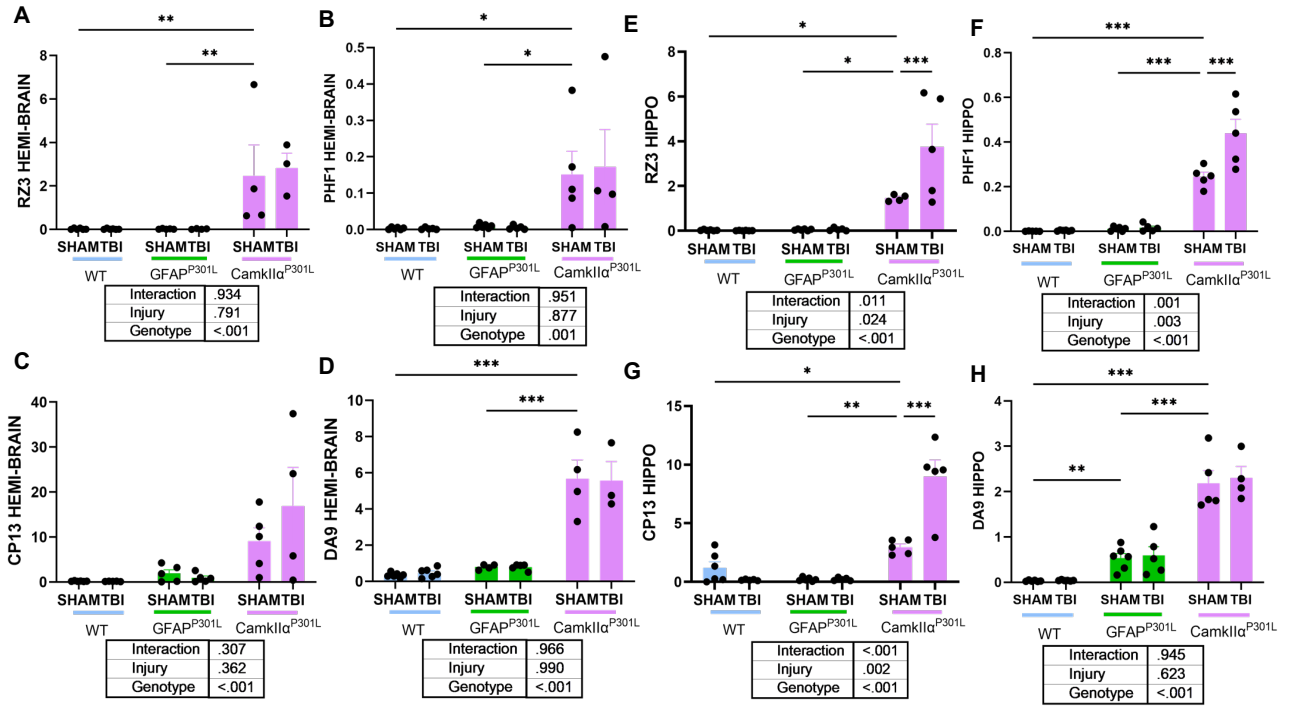

FIGURE 5. Changes in Tau species in WT, GFAP^{P301L} and Camk2^{P301L} mice at 3 months post-injury. Levels of RZ3, PHF1, CP13 and DA9 in the hemi-brain (*hemisphere minus the hippocampus*) (A-D) and Hippocampii (E-H) at 3 months post-last injury. Data analyzed by Two-Way ANOVA. Asterisks denote: *P<0.05; **P<0.01 and ***P<0.001 for post-hoc analyses.

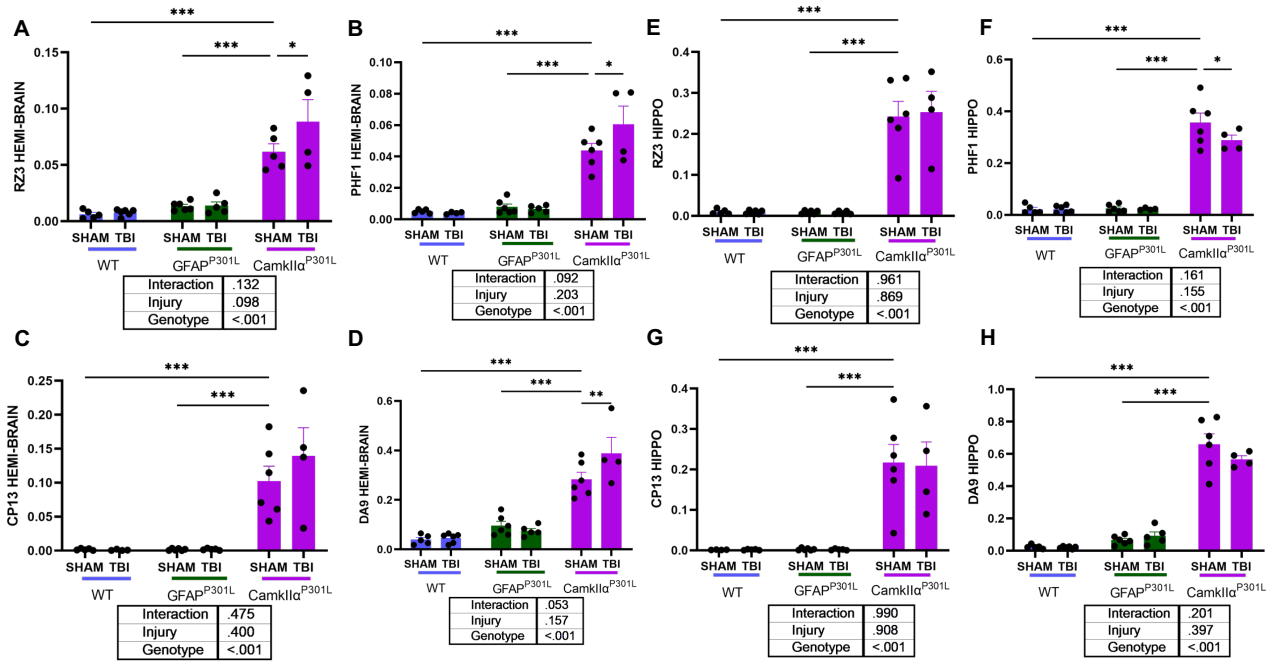

FIGURE 6. Changes in Tau species in WT, GFAP^{P301L} and Camk2^{P301L} mice at 6 months post-injury. Levels of RZ3, PHF1, CP13 and DA9 in the hemi-brain (*hemisphere minus the hippocampus*) (A-D) and Hippocampii (E-H) at 6 months post-last injury. Data analyzed by Two-Way ANOVA. Asterisks denote: *P<0.05; **P<0.01 and ***P<0.001 for post-hoc analyses.

Summary (immunoblotting)

Genotype effects

To investigate the influence of astroglial and neuronal tau on tau pathogenesis, we assessed the protein levels of several tau antibodies (RZ3, PHF1, CP13 and DA9) by immunoblotting in the hemi-brain (i.e., *hemisphere minus hippocampus*) and hippocampus of our mouse models.

At both 7 and 10 months of age, we observed a genotype effect by Two Way ANOVA for all 4 tau markers in the hemi-brain and hippocampus regions. This effect was mediated primarily by the significant and dramatic increase in all four tau markers in the CamkIIα^{P301L} cohort vs GFAP^{P301L} and WT cohorts (see **Figs 5 and 6**).

When we reanalyzed, the data using only the GFAP^{P301L} and WT cohorts, we noticed some genotype effects for CP13/PHF1/DA9 (hemi-brain) and RZ3/PHF1/DA9 (hippocampus) at 7 months of age (higher tau species in GFAP^{P301L} vs WT) – **see Fig 5**. Similarly, we also noticed genotype effects for RZ3/PHF1/DA9 (hemi-brain) and DA9 (hippocampus) at 10 months of age (higher tau species in GFAP^{P301L} vs WT) when we performed a Two-Way ANOVA on only the GFAP^{P301L} and WT cohorts – **see Fig 6**.

Injury effects in the 3 genotypes

At three months post-last injury, the biochemical analysis of all tau antibodies revealed a significant injury effect only in the CamkIIα^{P301L} cohort. This was typified by a significant TBI dependent increase in PHF1 and CP13 levels in the hippocampus (**Fig 5F, G**).

At six months post-last injury, we also revealed a significant injury effect only in the CamkIIα^{P301L} cohort. This was typified by a significant TBI dependent increase in RZ3, PHF1 and DA9 levels in the hemi-brain (**Fig 6A,B,D**). intriguingly, a significant TBI dependent decrease was observed in PHF1 levels in the hippocampus (**Fig 6F).**

Together these data demonstrates a significant increase in tau pathology in the CamkIIα^{P301L} cohort compared to both GFAP^{P301L} and WT cohorts. We also reveal TBI dependent increase in some tau species in the CamkIIα^{P301L} cohort. Although tau pathology levels in GFAP^{P301L} were much lower compared to CamkIIα^{P301L} cohort's it appeared that tau pathology was more pronounced in GFAP^{P301L} vs WT cohorts (albiet a mild increase).

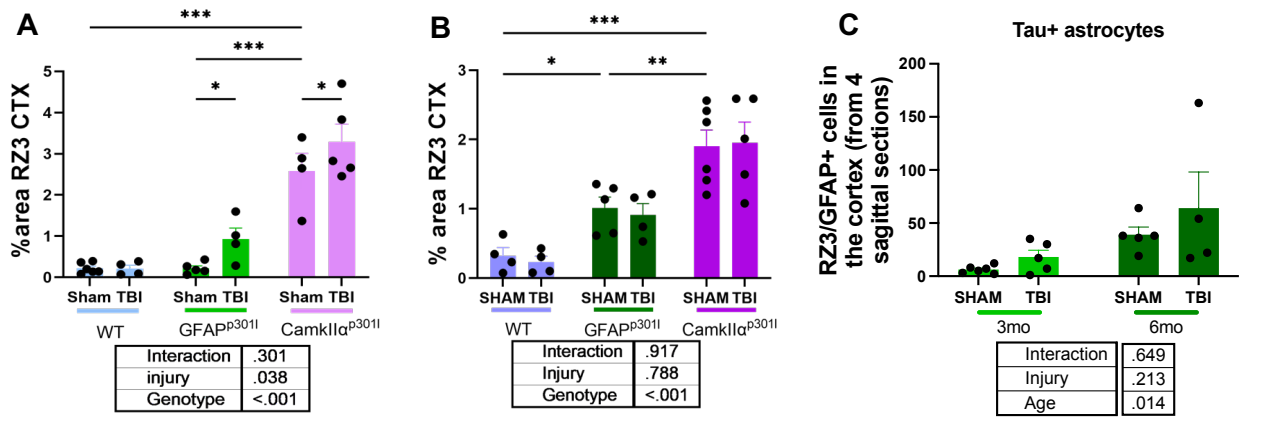

FIGURE 7. RZ3 immunoreactivity in the cortex of WT, GFAP^{P301L} and Camk2^{P301L} mice at 3- and 6-months post-injury. RZ3 percent area in the cortex at 3-months **(A)** and 6-months **(B)** post-last injury. RZ3/GFAP+ cells in the cortex from 4 serial sagittal sections at 3-months and 6-months post-last injury **(C)**. Data analyzed by Two-Way ANOVA. Asterisks denote: *P<0.05; **P<0.01 and ***P<0.001 for post-hoc analyses.

Summary (immunohistochemistry)

Genotype effects

To examine the effects of astroglial vs neuronal tau on tau phosphorylation in the cortex/regions beneath the impact site, we measured RZ3 (phosphorylated tau at threonine 231) immunoreactivity in the cortex.

At 7 mos of age, tau phosphorylation was not affected in the cortex of mice harboring tau-bearing astrocytes - GFAP^{P301L} vs WT; however, there was a 12-fold increase in CamkIIα^{P301L} mice compared to both WT and GFAP^{P301L} (**Fig. 7A**). In contrast, at 10 months of age, there was a significant 3-fold increase in tau phosphorylation in the GFAP^{P301L} compared to the WT (**Fig. 7B**). However, there was still a two-fold increase in RZ3 immunoreactivity in CamkIIα^{P301L} vs GFAP^{P301L} cohort (**Fig. 7B**).

We counted number of RZ3+ astrocytes stained with GFAP in the GFAP^{P301L} cohort and observed only an age dependent effect 6 months vs 3 month of age (**Fig. 7C**).

Injury effects in the 3 genotypes

Next, we investigated the effect of r-mTBI on tau phosphorylation under the cortical regions beneath the impact site, across all three genotypes.

At three months post-last injury, r-mTBI does not cause an increase in phosphorylated tau (p-tau) in the WT cohort; however, the presence of astroglial pathogenic tau (GFAP^{P301L} mice) and neuronal pathogenic tau (CamkIIα^{P301L}) result in a significant increase in p-tau immunoreactivity in the cortex compared to their respective sham counterparts (**Fig. 7A**).

Six months post-last injury, no significant TBI effect was observed across the three different mouse models (**Fig. 7B**).

Counts of RZ3+ astrocytes stained with GFAP in the GFAP^{P301L} cohort revealed no injury effect at both 3- and 6-months post-injury timepoints (**Fig. 7C**).

Correlation between astrocyte homeostatic markers and Tau pathology at 3 months post-injury in WT, GFAP^{P301L} and CAMK2A^{P301L} mice

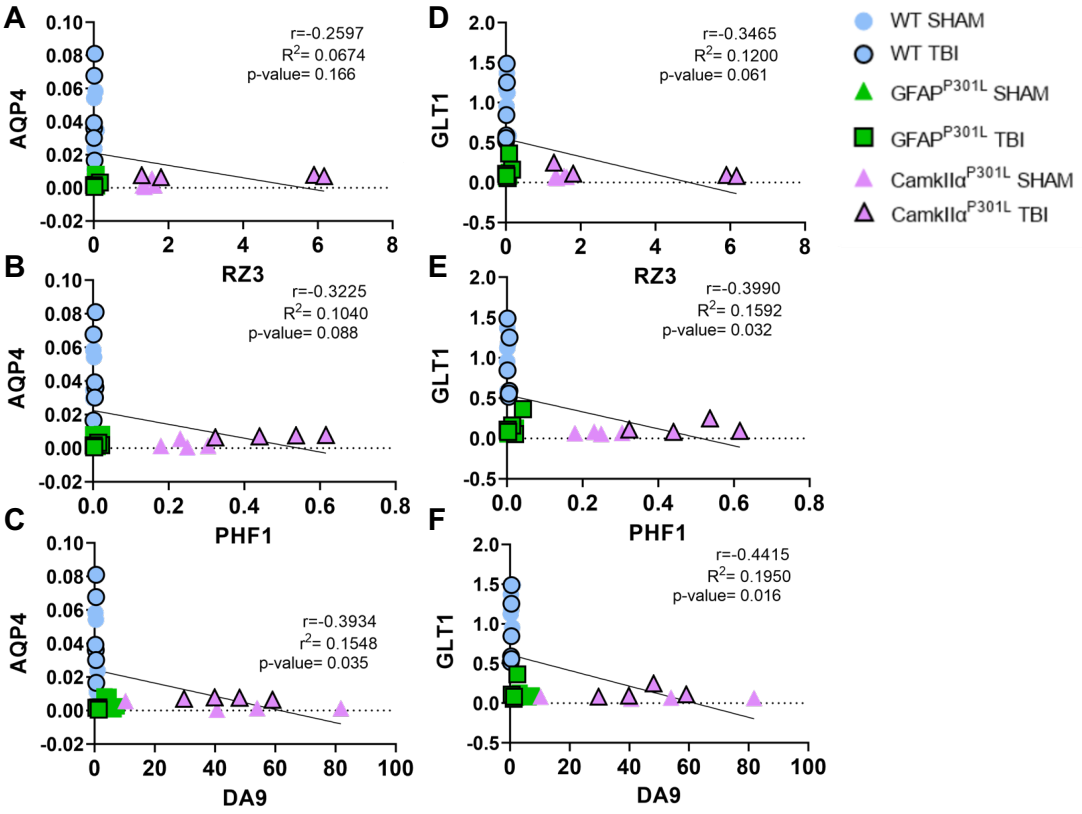

FIGURE 8. Correlation between AQP4/GLT1 and tau species in WT, GFAP^{P301L} and Camk2^{P301l} mice at 3 months post-injury. Correlation between AQP4/GLT1 vs RZ3(pTau-Thr231) [A,D], PHF1(pTau-Ser396/404) [B,E], DA9-total tau [C, F] in the hippocampus (HIPPO) at 3 months post-last injury. Data analyzed by Pearson's correlation.

Summary

Because we observed significant reduction in GLT1 and AQP4 at 7 months of age, we performed a Pearson correlation analyses between these two astrocyte homeostatic markers and our tau antibody markers – RZ3, PHF1 and DA9.

We reveal that GLT1 levels significantly and negatively correlated with PHF1 tau levels (**Fig 8E**).

We also reveal that both AQP4 and GLT1 levels significantly and negatively correlated with DA9 total tau levels (**Fig 8C, F**).

Synaptic integrity at 3 and 6 months post-injury in WT, GFAP^{P301L} and CAMK2A^{P301L} mice, and correlation with tau pathology

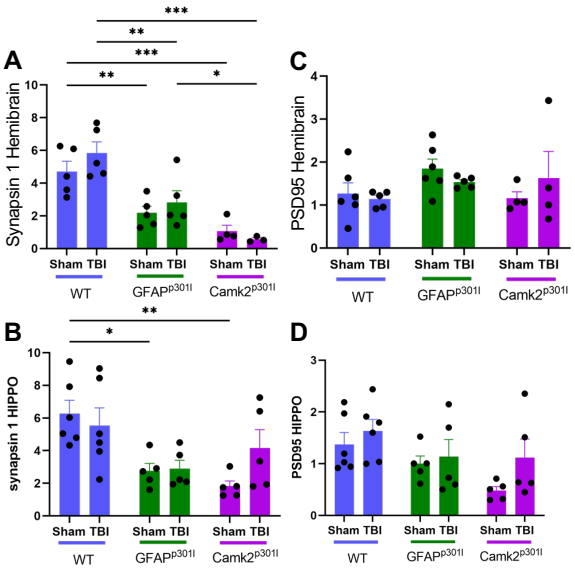

FIGURE 9. Synaptic integrity changes in WT, GFAP^{P301L} and Camk2^{P301l} mice at 3 mos post-injury. Levels of pre-synaptic synapsin1 in the hemibrain (*hemisphere minus the hippocampus*) (**A**) and hippocampus (HIPPO, **B**), and levels of post-synaptic density 95 (PSD95) in the hemibrain (**C**) and hippocampus (HIPPO, **D**) 3 months post-last injury. Data analyzed by Two-Way ANOVA. Asterisks denote: *P<0.05; **P<0.01 and ***P<0.001 for post-hoc analyses.

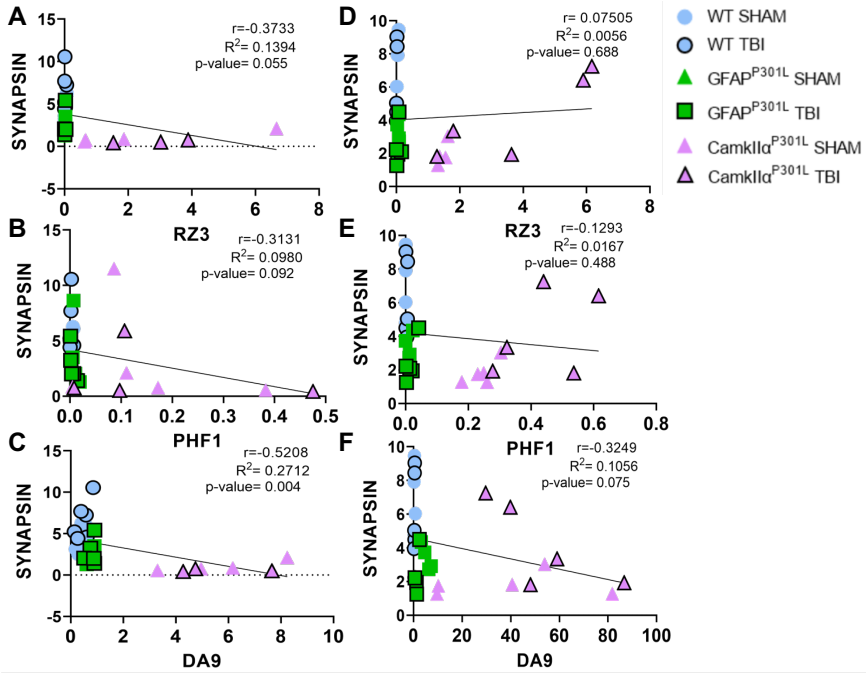

FIGURE 10. Correlation between synapsin 1 and tau species in WT, GFAP^{P301L} and Camk2^{P301l} mice at 3 months post-injury. Correlation between pre-synaptic synapsin1 vs RZ3(pTau-Thr231), PHF1(pTau-Ser396/404) and DA9-total tau in the hemibrain (*hemisphere minus the hippocampus*) (**A-C**) and hippocampus (HIPPO, **D-F**) 3 months post-last injury. Data analyzed by Pearson's correlation.

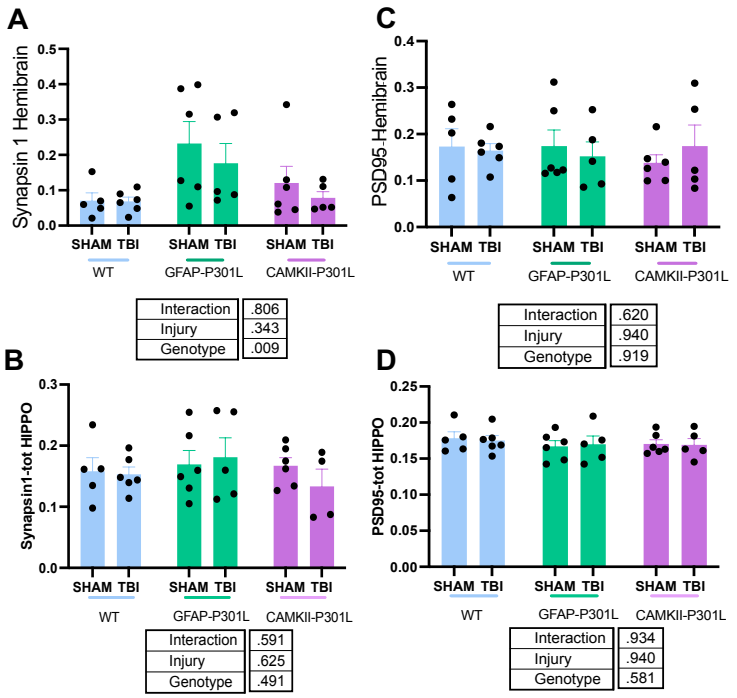

FIGURE 11. Synaptic integrity changes in WT, GFAP^{P301L} and Camk2^{P301l} mice at 6 mos post-injury. Levels of pre-synaptic synapsin1 in the hemibrain (*hemisphere minus the hippocampus*) **(A)** and hippocampus (HIPPO, **B**), and levels of post-synaptic density 95 (PSD95) in the hemibrain (**C**) and hippocampus (HIPPO, **D**) 6 months post-last injury. Data analyzed by Two-Way ANOVA. Asterisks denote: *P<0.05; **P<0.01 and ***P<0.001 for post-hoc analyses.

Summary

Genotype effects

To investigate whether the cell-type specific expression of pathogenic tau impairs synaptic integrity, we analyzed the protein levels of a pre-synaptic protein (synapsin 1) and a post-synaptic protein (PSD95) in hemibrain and hippocampal lysates of our mouse models.

At 7mo of age, the levels of the pre-synaptic marker - synapsin 1 - in the hemibrain of GFAP^{P301L} and CamkIIα^{P301L} mice revealed a ~2-fold and a 4.5-fold significant decrease, respectively, compared to WT (**Fig. 9A**). A similar decrease is observed in the hippocampus of GFAP^{P301L} and CamkIIα^{P301L} mice compared to WT (**Fig. 9B**). With respect to the levels of post-synaptic marker, PSD95, there were no significant differences in the hemi-brain or hippocampus across genotypes (**Fig. 9C, D**).

Given the notable changes in synapsin 1 levels at 7 mo of age, we performed a Pearson correlation analyses between synapsin 1 and our prominent tau markers – RZ3, PHF1 and DA9 in the hemibrain and hippocamps. Our analyses revealed that synapsin 1 levels was significantly negatively correlated with DA9 levels in the hemibrain (**Fig. 10C**).

At 10mo of age, we only observed a significant genotype effect in synapsin 1 levels in the hemibrain by Two Way Anova. This was accompanied by a significant 3-fold increase in the GFAP^{P301L} cohort compared to WT cohort (**Fig. 11A**). No changes in synapsin 1 levels were seen in the hippocampus (**Fig. 11B**). With respect to PSD95 levels, no difference was observed in the hemibrain or hippocampus across all three genotypes (**Fig. 11C, D**)

Injury effects in the 3 genotypes

To examine whether r-mTBI differentially impacts on synaptic integrity in our p301-tau bearing astrocyte vs neuronal models, we analyzed the protein levels of synapsin 1 and PSD95 in hemibrain and hippocampal lysates of these mouse models.

Three months post-last injury, no TBI-dependent changes in synapsin-1 or PSD95 were observed for any of the three genotypes in the hemi-brain or hippocampus (**Fig. 9**).

Similarly, at six months post-last injury, there was no TBI effect on the immunostaining of both synaptic markers in the hemi-brain or hippocampus across all three genotypes (**Fig. 11**).

Example of representative membranes from 3-month post-injury data presented above.

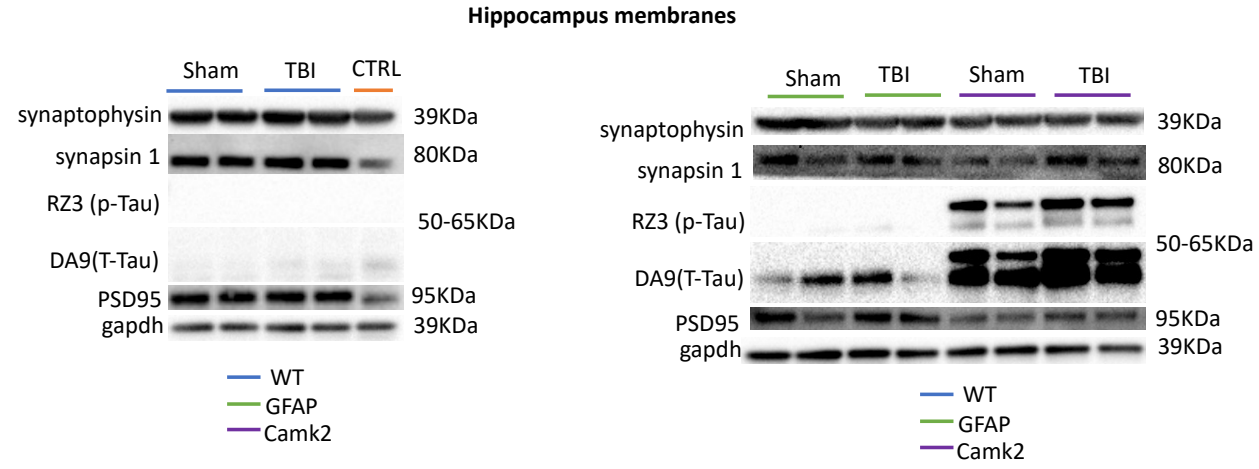

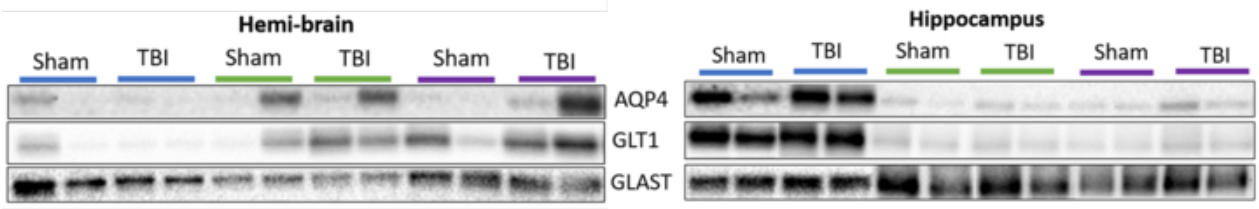

AIM 1 - Part Two: *Investigation of astroglial pathological lesions in autopsied brains from human TBI and ADRD cases.*

Major Task 1 (Sub task – 3)

Human TBI neuropathology of astrocyte lesions/markers

Table below shows group classification and history of de-identified patients used for the study.

Disease status	Age (yrs)	CDR	Plaque count	Braak Stage
Low CDR/Plaque AD	93.00	0.30	5.21	4.80
High CDR/Braak AD	76.91	2.36	18.14	6.00
Non Demented	79.64	0.09	0.15	1.00
Repetitive MTBI	61.86	-	N/A	N/A

Note: TBI patients presented here have evidence of 2 or more repetitive mild traumatic brain injuries with several decades post-survival.

Methods - Immunofluorescence protocol was used as previously detailed.

Qualitative images of markers analyzed are shown in Fig 1-3 below.

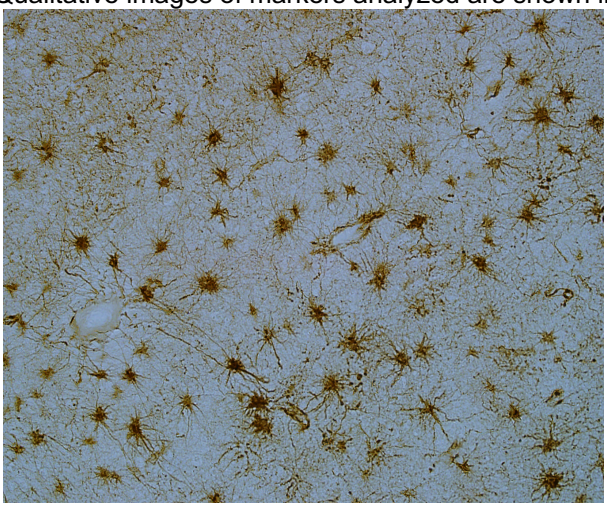

Fig.1 GFAP-DAB staining in human tissue. Magnification 20X.

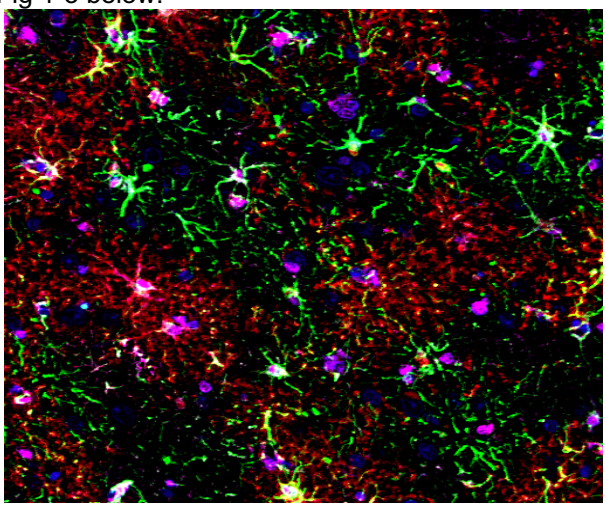

Fig.2 Immunofluorescence staining human tissue. GFAP (green), GLT1 (red) and S100b (purple). Magnification 20X.

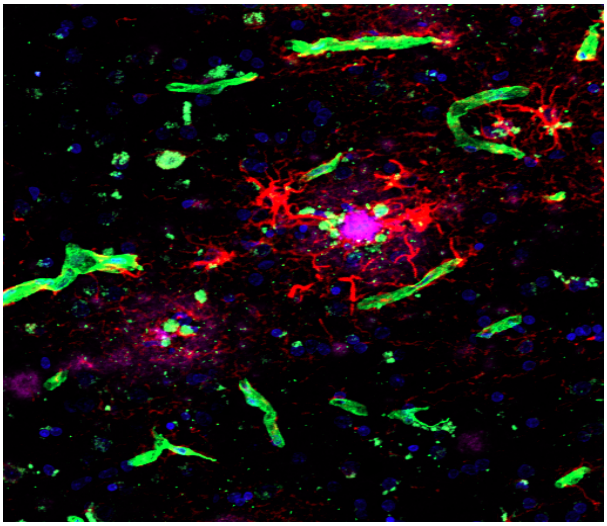

Fig.4 Immunofluorescence staining human tissue. GFAP (red), 4G8 (purple) and Laminin (green). Magnification 20X.

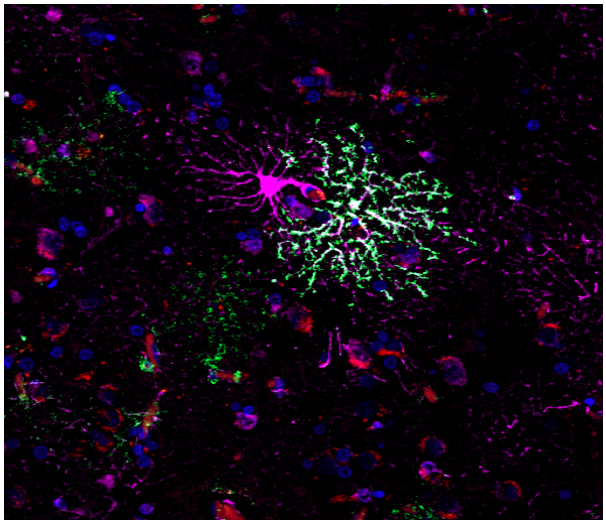

Fig.3 Immunofluorescence staining human tissue. GFAP (purple), MC1 (red) and AQ4 (green). Magnification 20X.

QUANTITATIVE ANALYSES

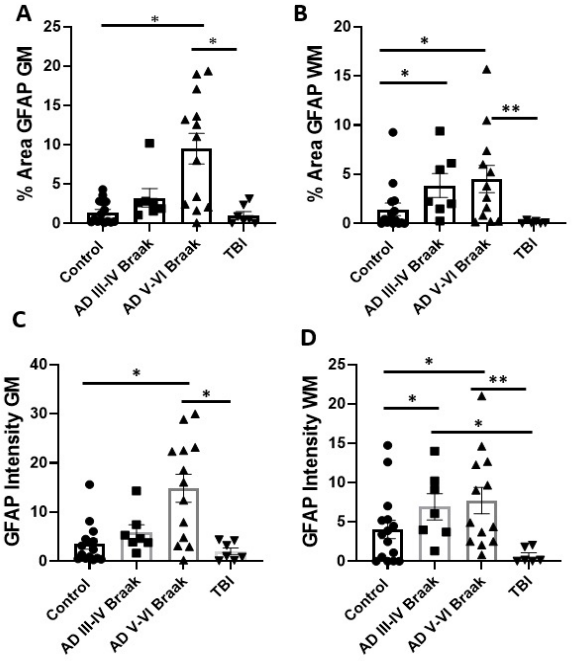

Figure 1. Percentage area [A-B] and intensity (au) [C-D] of positive Glial fibrillary acidic protein (GFAP) in grey (GM) and white matter (WM) of human brain derived from the medial temporal lobe. Control (n=15), AD Braak stages III-IV (n=7), AD Braak stages V-VI (n=13), and Traumatic brain injury (TBI) (n=7). p<0.03 *; p<0.002 **; p<0.001 ***. Data are presented as mean ±SEM.

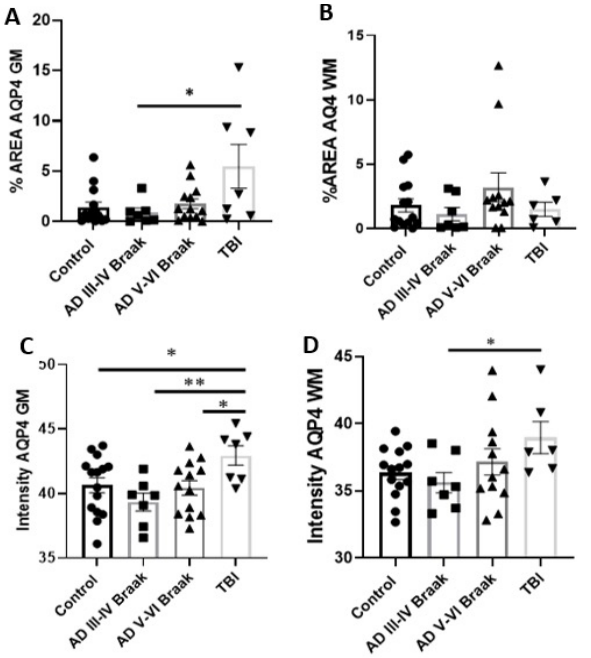

Figure 2. Percentage area [A-B] and intensity (au) [C-D] of Aquaporin 4 (AQ4) in grey (GM) and white matter (WM) of human brain derived from the medial temporal lobe. Control (n=15), AD Braak stages III-IV (n=7), AD Braak stages V-VI (n=13), and Traumatic brain injury (TBI) (n=7). p<0.03 *; p<0.002 **; p<0.001 ***. Data are presented as mean ±SEM.

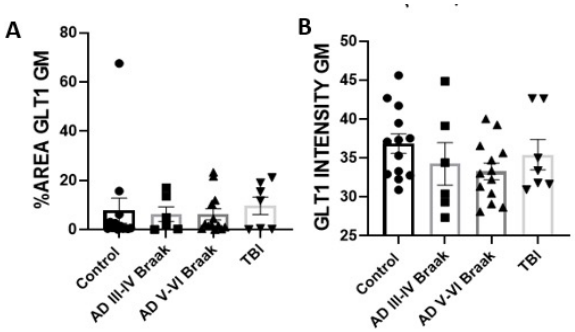

Figure 3. Percentage area [A] and intensity (au) [B] of Glutamate transporter 1 (GLT1) in grey matter (GM) of human brain derived from the medial temporal lobe. Control (n=15), AD Braak stages III-IV (n=7), AD Braak stages V-VI (n=13), and Traumatic brain injury (TBI) (n=7). p<0.03 *; p<0.002 **; p<0.001 ***. Data are presented as mean ±SEM.

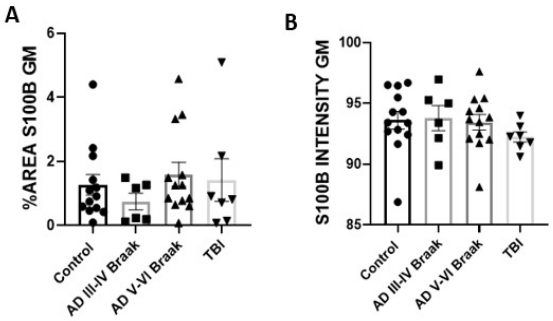

Figure 4. Percentage area [A] and intensity (au) [B] of S100B in grey matter (GM) of human brain derived from the medial temporal lobe. Control (n=15), AD Braak stages III-IV (n=7), AD Braak stages V-VI (n=13), and Traumatic brain injury (TBI) (n=7). p<0.03 *; p<0.002 **; p<0.001 ***. Data are presented as mean ±SEM.

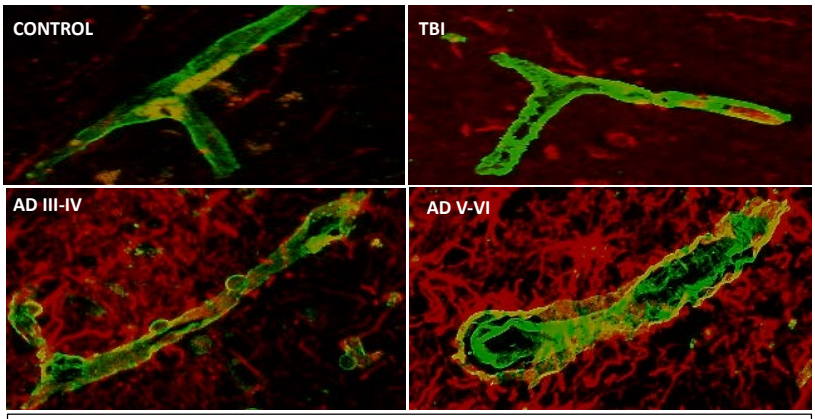

Reactive astrocytes covering blood vessels: Astrocytes (red) covering surface of blood vessels stained by laminin (green) in control (n=13), AD III-IV Braak stage (n=6), AD V-VI (n=13), and TBI (n=6) cases.

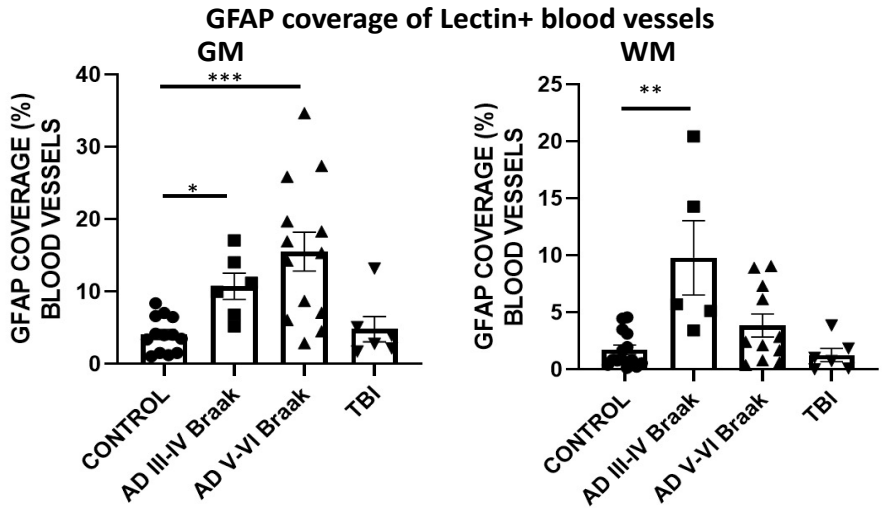

Figure 5. GFAP coverage of Lectin+ blood vessels in the grey and white matter of human brain from the medial temporal lobe. Control (n=15), AD Braak stages III-IV (n=7), AD Braak stages V-VI (n=13), and Traumatic brain injury (TBI) (n=7). $p<0.03$ *; $p<0.002$ **; $p<0.001$ ***. Data are presented as mean ±SEM.

Summary

>GFAP levels were significantly upregulated in AD brains but downregulated in TBI brains compared to healthy non-demented controls (**Figure 1**).

>AQ4 levels were upregulated in TBI compared to healthy control cases (**Figure 2**).

>No significant changes were observed in S100beta and GLT1 levels in TBI or AD cases compared to non-demented controls (**Figure 3 and 4**).

>There was a greater area of astrocytic coverage around blood vessels in the brains of AD cases vs non-demented control (**Figure 5**).

Given the disparate finding in this human autopsy TBI cohorts, we sought for a different TBI cohort with documented neuropathological changes from the Boston Brain Bank for our analyses by laser capture microdissection and gene array of GFAP+ astrocytes.

AIM 2: Evaluated pathobiological effects of reactive/injured astrocytes derived from mouse models in Aim 1, on the induction of neurodegeneration.

Major Task 2 (Sub task – 4)

Priming studies: Effect of exposing r-mTBI vs sham astrocytes from WT-non-carriers, GFAP^{P301L} and CAMK2A^{P301L} mice to LPS.

Method: WT-non-carriers, GFAP^{P301L} and CAMK2A^{P301L} mice were exposed to r-mTBI (N=3) and sham injury(N=3). Brains were collected and processed under sterilized conditions. Glial cells were isolated from brain homogenate using percoll gradient centrifugation and co-cultured at 37ºC for a few weeks. Astrocytes were separated from microglia through shaking at 37ºC for three hours. Isolated astrocytes were cultured for another week until 80% confluency was reached, during these processes astrocyte conditioned media (ACM) was collected and frozen until required for the subsequent study. TBI and sham astrocytes were exposed to LPS for 8hrs and frozen for further probing. Protein was extracted from cell lysates of astrocytes, run in a gel, and probed for specific markers using western blotting. ACM was used for exposure to microglial cell lines in subsequent experiments below.

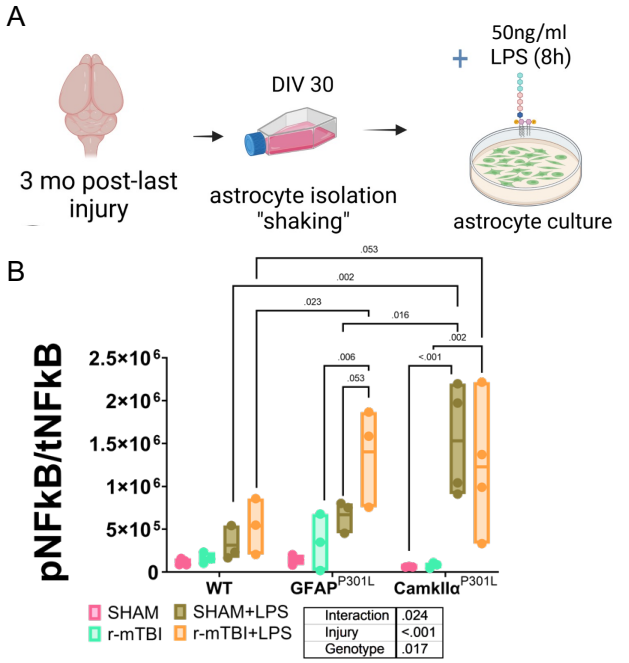

Figure 1: Primary Astrocyte NFkB response from WT, GFAP-P301L and CAMK2A-P301L r-mTBI vs sham mice at baseline and following exposure to LPS. (A) schematic of study. (B) Densitometry values for pNFkB/total-NFkB levels.

SUMMARY OF RESULTS

Primary astrocytes harvested from GFAP^{p301l}, CAMK2A^{p301l} and non-carrier control r-mTBI and sham mice were exposed to 50ng/ml of LPS for 8h (**Fig. 1A**).
Phosphorylated NFκB (p NFκB) was used to evaluate cellular activation/response (**Fig. 1B**). In general, astrocytes exposed to LPS showed increased pNFκB levels compared to their baseline levels, regardless of their genotype (non-carrier or GFAP^{p301l} or CAMK2A^{p301l}) or condition (Sham or TBI). This effect was however only significant in the GFAP^{p301l} or CAMK2A^{p301l} cohorts. Moreover the LPS effect in GFAP^{p301l} or CAMK2A^{p301l} cohorts was significantly increased compared to WT non-carrier cohorts (irrespective of sham or TBI condition). A trend towards increase in LPS exposed r-mTBI vs sham levels of pNFkB was observed

in the GFAP^{p301l} cohorts (P=0.053). It is important to highlight that astrocytes extracted from TBI GFAP^{p301l} mice exhibited a very pronounced cellular activation compared to its sham counterpart and non-carrier/CAMK2A^{p301l} cohorts. These results provide an insight to the potential detrimental role of tau astrogliopathy on astrocyte homeostatic function, typified here by a primed and augmented response to the exposure of inflammatory stimuli.

Major Task 3 (Sub task – 2b)

Analyses of secretome from r-mTBI vs sham astrocytes obtained from WT-non-carriers, GFAP^{P301L} and CAMK2A^{P301L} mice.

Cytokine profiles of r-mTBI vs sham astrocyte secretome obtained from WT, GFAP^{p301l} and CAMK2a-P301L models. Analyses was conducted by **MSD ELISA plate (10-Plex):** IL-1β, IL-10, TNFα, IFNγ, IL-2, IL-4, IL-5, IL-6, IL-12p70, KCGRO (IL-8)

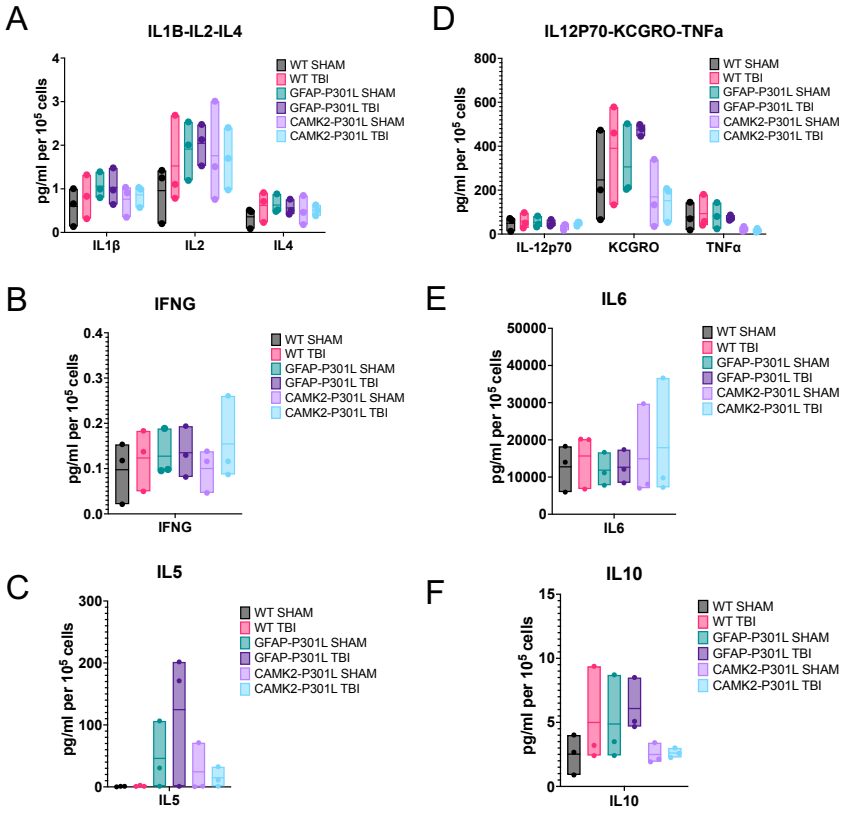

Figure 2: Primary astrocyte secretome (cytokine) profiles from WT, GFAP-P301L and CAMK2A-P301L r-mTBI vs sham mice. A-F shows ELISA concentration levels in the media for IL1B, IL2, IL4, IL12p70/IL8, TNFa, IFNy, IL6, IL15 and IL10.

SUMMARY

Analyses of cytokines in the secretomes of TBI vs sham astrocyte conditioned media (ACM) collected from the three mouse models revealed no statistically significant changes between the different groups.

Notably, we did observe some trends in the genotype effects.
For example, a trend towards increase in IL5 was observed in GFAP^{P301L} and CAMK2A^{P301L} ACM compared to WT-non carrier ACM, irrespective of injury group.

Likewise, a trend towards decrease in IL10 and KCGRO (IL8) and TNFa was observed in CAMK2A^{P301L} ACM compared to GFAP^{P301L} ACM, irrespective of injury group.

Major Task 2 (Sub task – 4)

Ex vivo experiment to determine pathobiological effects of exposing conditioned media derived from adult astrocyte cultures obtained from our transgenic TBI models, and their impact on healthy microglial cell populations.

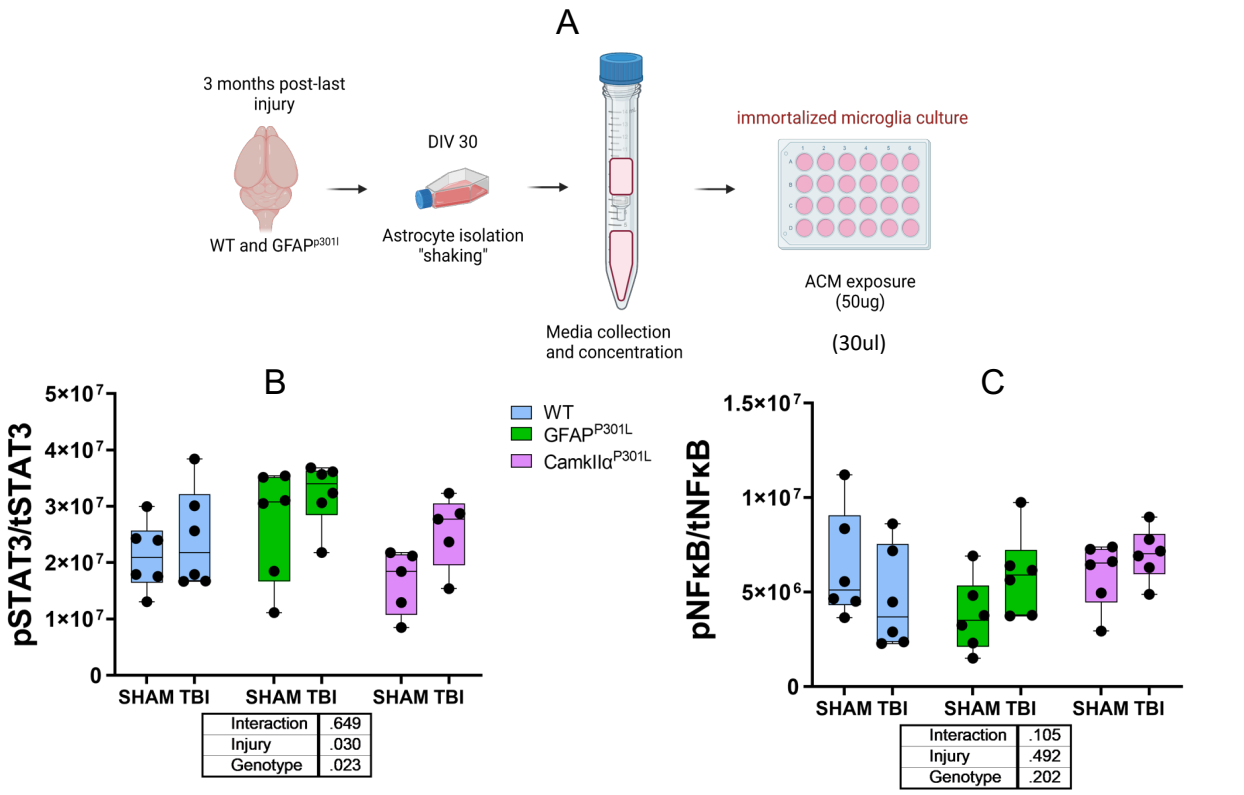

Figure 3: pNFkB/pSTAT3 inflammatory response of microglial cell lines exposed to primary astrocyte secretome obtained from WT, GFAP-P301L and CAMK2A-P301L r-mTBI/Sham mice. (A) schematic representation of the study. (B, C) Densitometry values for pSTAT3/total-STAT3 and pNFkB/total-NFkB levels.

Summary

We collected astrocyte media from TBI vs sham GFAP^{P301L}, CAMK2A^{P301L} and WT-non carrier primary adult astrocyte cultures and exposed them to a healthy mouse microglial cell line (IMG microglia) for 30 mins to investigate the genotype effect and injury effect of astrocyte conditioned media (ACM) on microglial proinflammatory response (i.e., pSTAT3/tSTAT3 and pNFkB/tNFkB levels).

An injury and genotype effect were observed for pSTAT3/tSTAT3 levels. However, no significant post-hoc differences were observed. Notably there was a trend towards increase in r-mTBI vs sham pSTAT3/tSTAT3 levels in the CAMK2A^{P301L} cohort. No injury or genotype effect was observed in pNFkB/tNFkB levels.

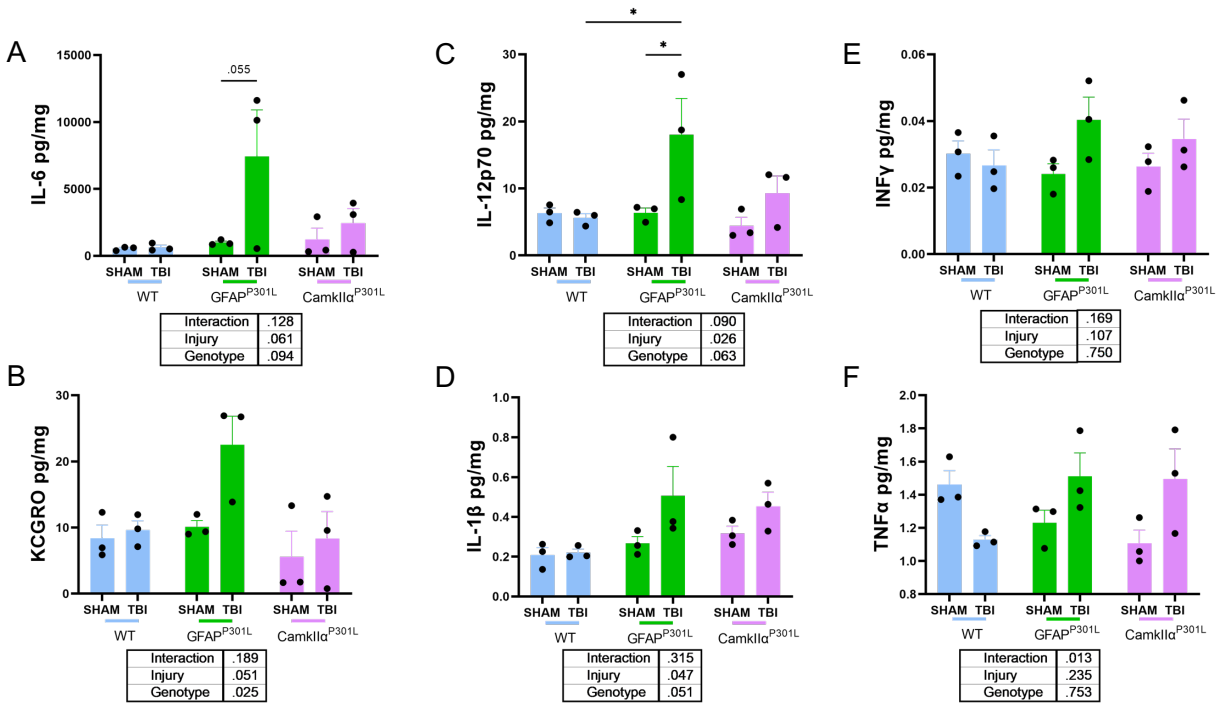

Figure 4: Cytokine levels in the media of microglial cell lines exposed to primary astrocyte secretome obtained from WT, GFAP-P301L and CAMK2A-P301L r-mTBI/Sham mice. A-F shows ELISA concentration levels in the media for IL6,IL12p70, IFNy, IL8, IL1B and TNFa. Asterisks denote: *P<0.05

Summary

We continued our investigation of the genotype and injury effects of astrocyte conditioned media (ACM) on microglial proinflammatory response by probing cytokines released into the media.

Although the study was underpowered, we observed an injury effect on IL1B and IL-12p70 levels (**Fig 4C,D**).
A genotype effect was observed for KCGRO (or IL8) – **Fig 4B**.
A genotype and interaction effect were noted for TNFalpha – **Fig 4F**.
Post-hoc analyses only revealed a statistical difference in IL-12P70 levels in the r-mTBI vs sham GFAP^{P301L} cohort (**Fig 4C**). A trend towards increase was also observed in the same cohort for IL6, IL1B, IL8, IFNy and TNFapha (**Fig 4A-F**).

Major Task 2 (Sub task – 6)

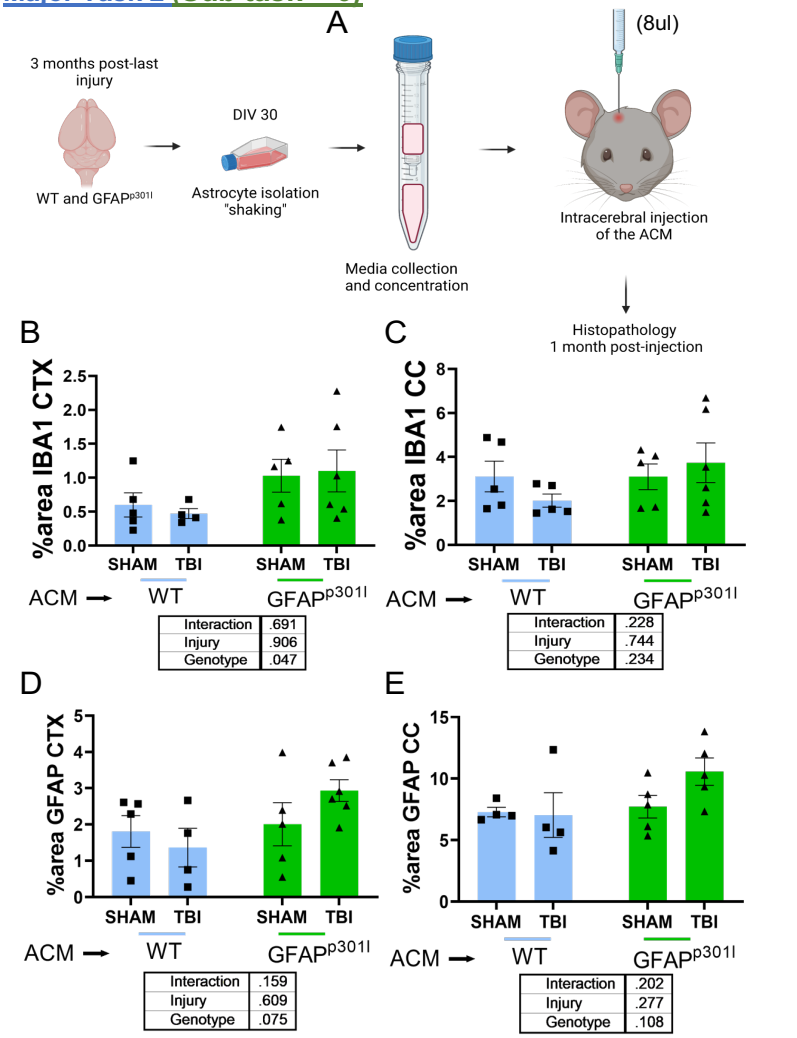

Figure 5: Astroglial and microglial reactivity following intracerebral (IC) injection of primary astrocyte secretome obtained from WT-non carriers and GFAP-P301L r-mTBI/Sham mice into naïve recipient WT mice. (A) schematic representation of the study. IBA1 (B, C) and GFAP (D,E) immunoreactivity in the cortex and corpus callosum of IC injected recipient mice.

Summary

We collected astrocyte media from TBI vs sham GFAP^{P301L} and WT-non carrier primary adult astrocyte cultures and intracerebrally (IC) injected them into naïve WT mice to investigate the genotype effect and injury effect of astrocyte conditioned media (ACM) on promoting proinflammatory response (i.e., GFAP and IBA1 immunoreactivity in the cortex and corpus callosum levels). Analyses were performed 3weeks after IC injections.

A genotype effect (↑ GFAP^{P301L} vs WT-non carrier) was observed for IBA1 immunostaining in the cortex – **Fig 5A**. No other significant effects were observed. A trend towards increase in GFAP was observed in the cortex and corpus callosum of r-mTBI vs sham GFAP^{P301L} cohorts (**Fig 5D, E)**.

AIM 3 - Part One: Generation of single cell genomic profiles in different populations of astrocytes obtained from the same mouse models described in Aim 1.

Major Task 3 (Sub task – 2a)

METHODOLOGY

Mouse Transcriptomics

Astocytes cells were isolated using enzymatic degradation and percoll gradient centrifugation followed by magnetic assisted cell sorting (MACS). **HiSeq sequencing:** RNA samples were prepared using the Qiagen RNeasy Kit, quantified and checked for integrity. RNA library preparation with PolyA and sequencing reactions was conducted at Genewiz (South Plainfield, NJ). The NEBNext Ultra RNA Library Prep Kit for Illumina was used for RNAseq library preparations. Briefly, mRNA was first enriched with Oligod(T) beads and fragmented, with the 1st and 2nd strand cDNA subsequently synthesized. cDNA fragments were end repaired and adenylated, and universal adaptor ligated to fragments, followed by index addition and library enrichment with limited cycle PCR. Validated and quantified sequencing libraries were multiplexed and clustered on one lane of a Flow Cell. After clustering, the flow cell was loaded on the Illumina instrument, with samples sequenced using a 2×150 Paired End configuration. Raw sequence data generated from Illumina HiSeq was converted into Fastq files and de-multiplexed. **Bioinformatic analyses**: After quality checking of Fastq files, sequence reads were trimmed, and mapped to the Mus musculus GRCm38 reference genome. Data were inspected for outlying samples using unsupervised hierarchical clustering and principal component analysis. Combat batch correction was applied to combine the datasets and reduce systematic sources of variability. Differential gene expression analysis: This was conducted to determine relationships between gene expression levels and injury status. The covariates were included in all models to adjust for any potential confounding influence on gene expression between main group effects. This was conducted using the Wald test (in DESeq2Genes with FDR adj p<0.05 and log2 fold changes >1.3 were classified as differentially expressed genes (DEG).). Gene ontology/ pathway analyses: This was used to identify pathways to which significantly regulated genes belong, including their cell-type origin, cellular components, molecular functions and canonical signaling pathways. We conducted enrichment tests for DEGs using hypergeometric statistic, controlling for background set enrichment and multiple testing, or a leading-edge rank-based method. Upstream regulator analysis: This was performed in the Ingenuity Pathway Analysis software to predict upstream regulators driving the observed DEG's.

Mouse Transcriptomics (schematic)

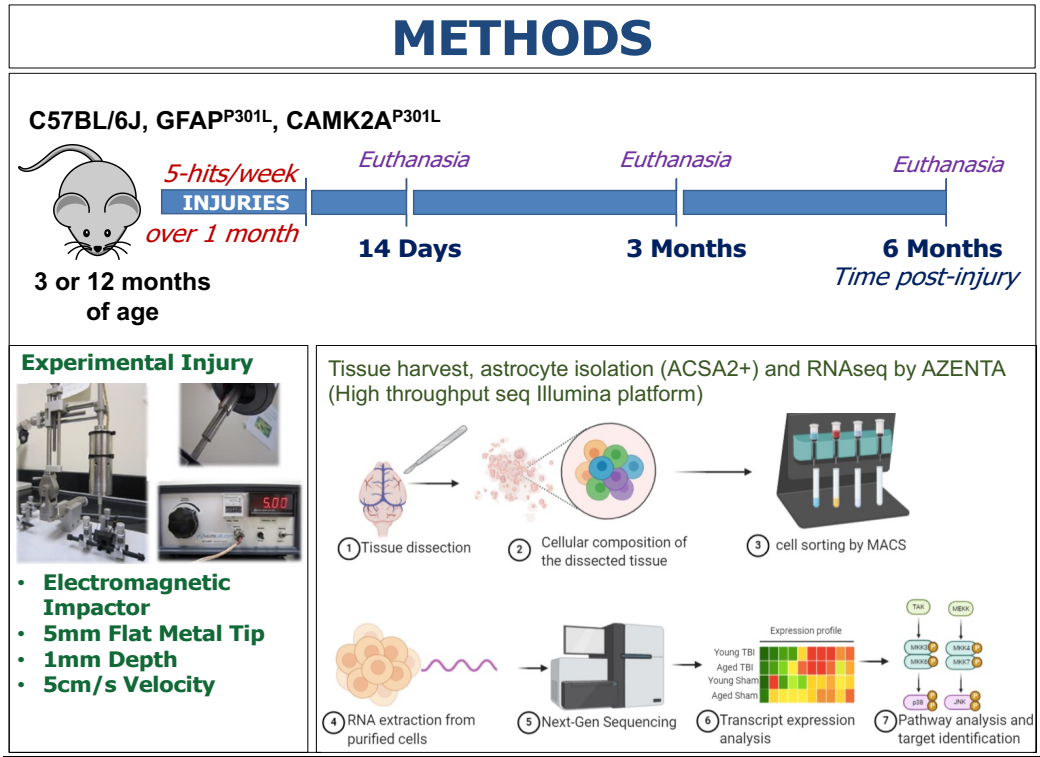

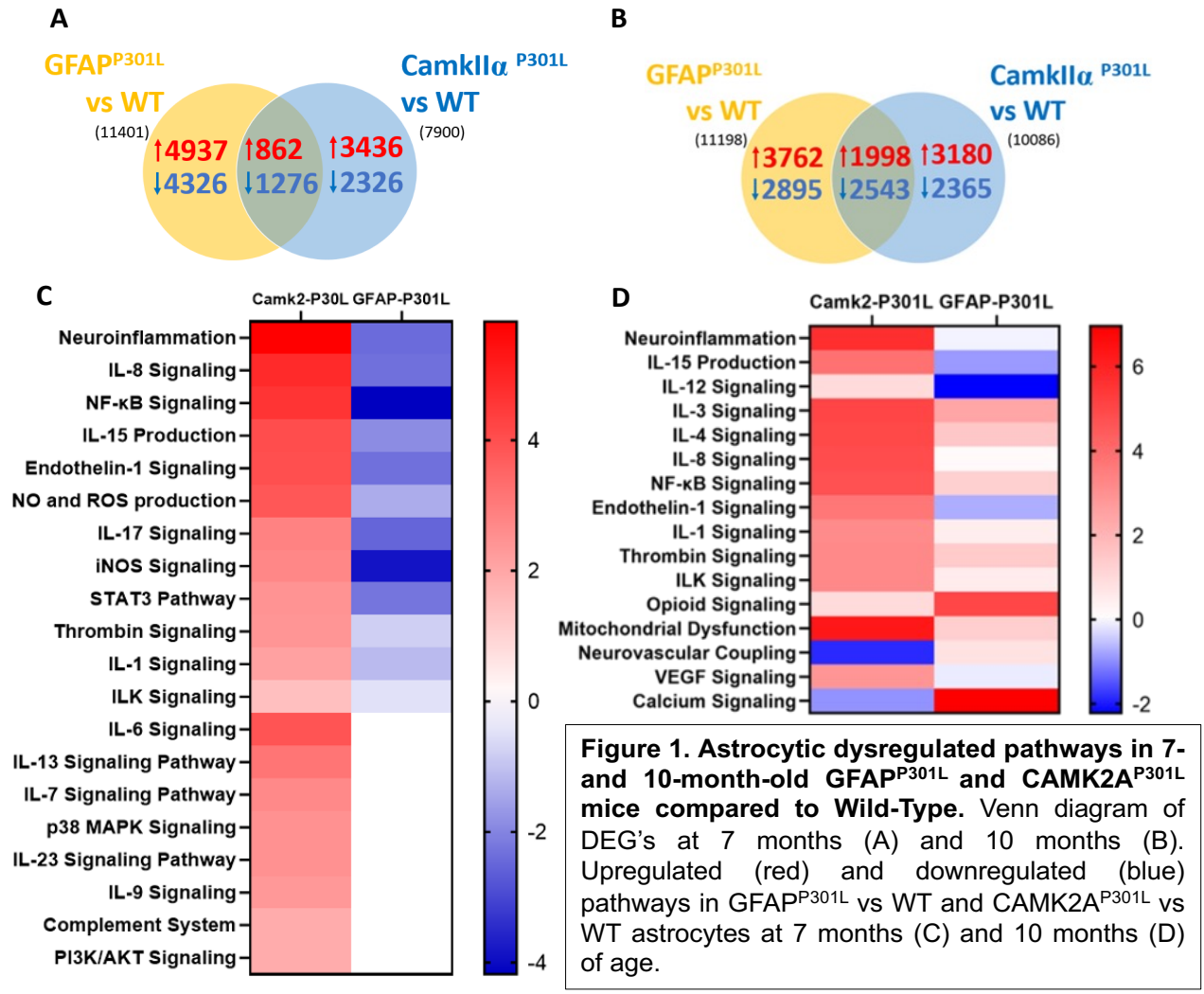

Figure 1. Astrocytic dysregulated pathways in 7- and 10-month-old GFAP^{P301L} and CAMK2A^{P301L} mice compared to Wild-Type. Venn diagram of DEG's at 7 months (A) and 10 months (B). Upregulated (red) and downregulated (blue) pathways in GFAP^{P301L} vs WT and CAMK2A^{P301L} vs WT astrocytes at 7 months (C) and 10 months (D) of age.

Summary

To determine the changes in astrocytic gene expression across our mouse models in response to astroglial or neuronal tau, we extracted the RNA from astrocytes isolated at 7mo and 10mo of age. We determined the number of genes that are differentially expressed in astrocytes in three mouse models (WT, GFAP^{P301L,} and CamkIIα^{P301L}) at both time points. Considering only significantly altered genes (adjusted p-value<0.05), we identified that at **7mo of age**, the presence of tau within astrocytes of our GFAP^{P301L} model induces the dysregulation of 11401 astroglial genes (5799 upregulated and 5602 downregulated) compared to WT, while the presence of neuronal tau in the brain causes the dysregulation of 7900 genes (4298 upregulated and 3602 downregulated) in CamkIIα ^{P301} astrocytes compared to WT astrocytes (**Fig. 1A**). To investigate if there are genes that are commonly dysregulated in astrocytes expressing pathogenic tau vs those exposed to neuronal derived pathogenic tau, we compared the dysregulated genes (DEGs) obtained from GFAP vs WT and CamkII vs WT astrocytes. It was observed that there was a dysregulation of 2138 common genes (862 upregulated and 1276 downregulated) in both group comparisons.

Next, we performed pathway enrichment analysis on the significantly dysregulated genes. Interestingly, two opposing profiles were observed. At **7mo of age**, tau-bearing astrocytes show an immunosuppressed phenotype, characterized by the downregulation of *interleukin signaling (IL-8, IL-15, IL17, IL-1), NFKB and STAT3 signaling* as well as production of *nitric oxide (NO) and reactive oxygen species (ROS)* (**Fig. 1C**) compared to WT astrocytes. On the contrary, CamkIIα^{P301L} astrocytes showed the upregulation of the above-mentioned pathways when compared to WT astrocytes. Other important pathways identified in GFAP^{P301L} astrocytes included the upregulation of calcium signaling and antioxidant action of ascorbic acid.

CamkIIα^{P301L} astrocytes also exhibit downregulation of neurovascular coupling and antioxidant action and the upregulation of ephrin-B signaling. Overall, changes seen in our mouse models suggest that GFAP^{P301L} astrocytes have an immunosuppressed phenotype and engage in neuroprotective function, while CamkIIα^{P301L} astrocytes have a proinflammatory phenotype and inability to provide antioxidant defense. Additionally, enriched pathway analysis identified that the 2138 genes that GFAP^{P301L} and CamkIIα^{P301L} have in common, were associated with the upregulation of chemokine signaling, CREB signaling to neurons, and synaptogenesis; and the downregulated inhibition of matrix metalloproteases which may indicate activation of common neuroprotective/neurorestorative pathways against the pathogenic tau environment.

At **10 mo of age**, we identified that GFAP^{P301L} astrocytes had 11198 DEGs (5759 upregulated and 5439 downregulated) compared to WT (**Fig 1B**). Those genes were found to drive the dysregulation of 234 pathways including the upregulation of calcium signaling, glutamate receptor signaling, mitochondrial dysfunction as well as a sustained immunosuppressed phenotype. At **10 mo of age**, we identified that CAMK2A^{P301L} astrocytes had 10086 DEGs (5178 upregulated and 4908 downregulated) compared to WT. Pathway analyses revealed upregulation of numerous inflammatory pathways (IL15, IL1, IL3, IL8, NFkB signaling) and thrombin signaling, an increase in mitochondrial dysfunction, and decrease in calcium signaling (**Fig 1D**).

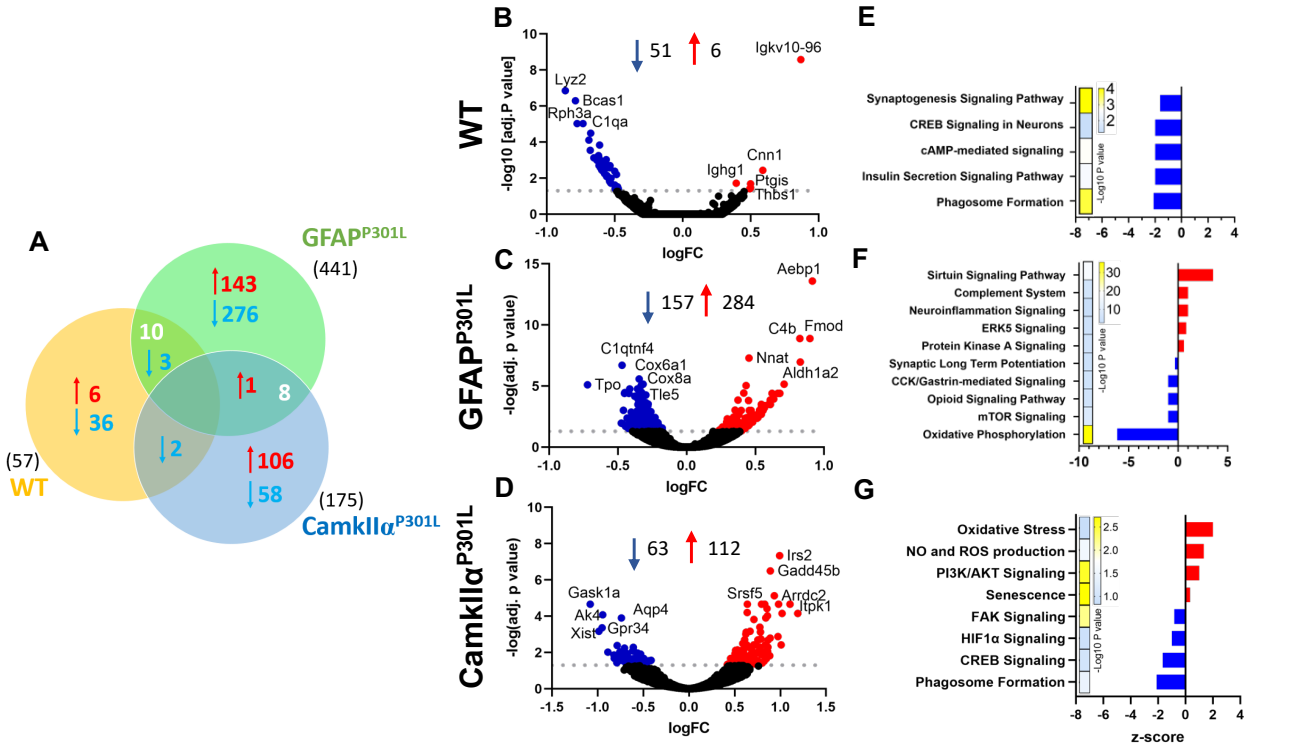

Figure 2. Differentially expressed genes (DEG's) and dysregulated pathways in ACSA2+ astrocytes isolated from young WT, GFAP^{P301L} and CAMK2^{P301L} r-mTBI vs sham mice at 3 months post-injury. Venn diagram showing the overlap of TBI-dependent astrocytic DEGs across the 3 different genotypes (A). Volcano plot of differentially expressed genes (DEGs) in WT (B), GFAP^{P301L} (C) and CAMK2^{P301L} (D) r-mTBI vs sham astrocytes at 3 months post-last injury. Upregulated (red) and downregulated (blue) pathways in WT (E), GFAP^{P301L} (F) and CAMK2^{P301L} (G) r-mTBI vs sham astrocytes at 3 months post-last injury. Threshold for obtaining the DEGs: adj. p-value≥0.05 with its respective –log value≥1.3. N=6 mice/group (N=3 technical replicates)

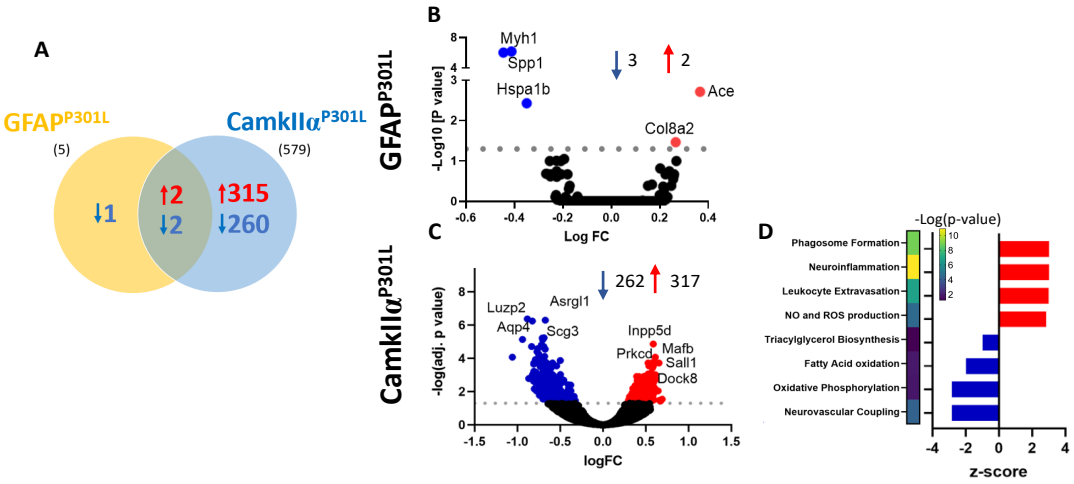

Figure 3. Differentially expressed genes (DEG's) and dysregulated pathways in ACSA2+ astrocytes isolated from young GFAP^{P301L} and CAMK2^{P301L} r-mTBI vs sham mice at 6 months post-injury. Venn diagram showing the overlap of TBI-dependent astrocytic DEGs across the 2 different genotypes (A). Volcano plot of differentially expressed genes (DEGs) in GFAP^{P301L} (B) and CAMK2^{P301L} (C) r-mTBI vs sham astrocytes at 3 months post-last injury. Upregulated (red) and downregulated (blue) pathways in CAMK2^{P301L} (D) r-mTBI vs sham astrocytes at 3 months post-last injury. No pathways were detected from the GFAP^{P301L} cohort due to the low DEG number identified. Threshold for obtaining the DEGs: adj. p-value≥0.05 with its respective –log value≥1.3. N=6 mice/group (N=3 technical replicates)

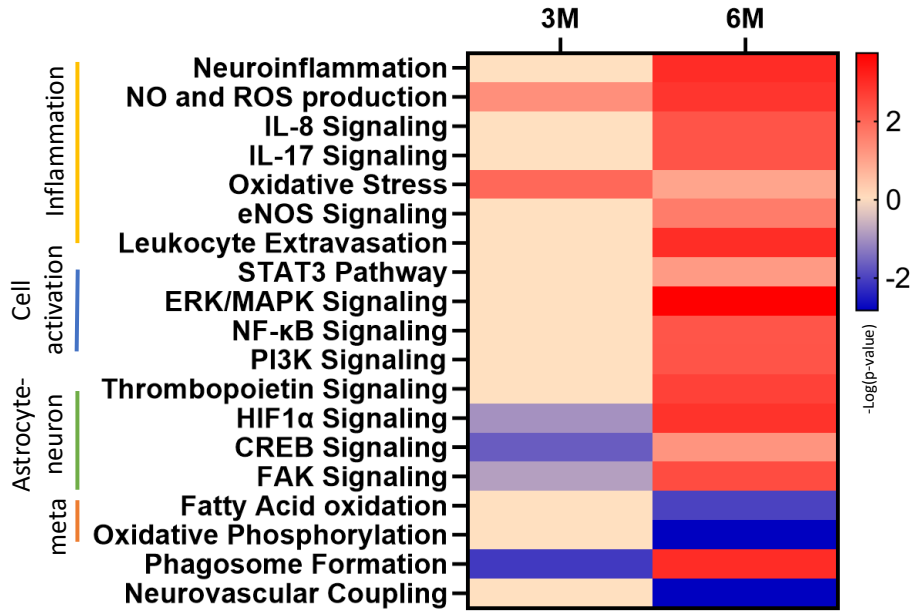

Figure 4. Comparative analysis of astrocytic dysregulated pathways in Camk2^{P301L} 3 and 6 months after rmTBI. 3M and 6M = 3 and 6 months post-last injury. Threshold p-value ≥0.05 with its respective –log value≥1.3.

Summary

Next, the changes in astrocytic gene expression across our mouse models in response to r-mTBI were evaluated.

Three months post-last injury, r-mTBI caused the dysregulated expression of 57 genes (51 downregulated and 6 upregulated) in WT, 175 genes (63 downregulated and 112 upregulated) in CamkIIα^{P301L}, and 441 genes (157 downregulated and 284 upregulated) in the GFAP^{P301L} mice (**Fig. 2A-D**). This demonstrates that the presence of endogenous p301l-human tau in astrocytes causes greater transcriptomics gene dysregulation in response to r-mTBI compared to the exposure of astrocytes to exogenous neuronal tau in the CamkIIα^{P301L} or when pathogenic human tau presence is null in WT mice. Additionally, no common TBI-gene alterations were identified across the genotypes (**Fig. 2A**).

Next, we performed pathway enrichment analysis on the significantly dysregulated genes. In the WT cohort, the 57 significantly regulated genes were analyzed by IPA to predict the functional consequences of their dysregulation, and 6 significantly modulated pathways were identified. These include *phagosome formation, insulin secretion, c-AMP signaling, and synaptogenesis signaling* (**Fig. 2E**), all of them downregulated. Regarding the GFAP^{P301L} cohort, 441 DEG's mapped to 52 significant pathways including the downregulation of *oxidative phosphorylation*, *synaptic long-term potentiation*, and *opioid signaling*; and the upregulation of *neuroinflammation*, *complement system signaling*, and *ERK5-mediated cell activation* (**Fig. 2F**). In the CamkIIα^{P301L} cohort, 175 differentially expressed genes (DEG's) were mapped to 17 significant pathways. Those include the downregulation of *phagosome formation and neuroprotective erythropoietin signaling*, the upregulation of *nitric oxide and reactive oxygen species production*, and *senescence* (**Fig. 2G**).

⇒*These datasets reveal that in our p301-tau bearing astrocyte model, r-mTBI elicits more pronounced changes that compromise mitochondrial functioning and neuronal supportive mechanisms; and favors a pro-inflammatory state compared to that observed in WT and CamkIIα^{P301L}.*

Six months post-last injury, r-mTBI caused the dysregulated expression of 555 genes (298 downregulated and 257 upregulated) in CamkIIα^{P301L} astrocytes, and 5 genes (3 downregulated and 2 upregulated) in the GFAP^{P301L} astrocytes (**Fig. 3A-C**). It is important to mention that data from the WT cohort has been omitted due to technical issues with the r-mTBI samples. Similar to the three-month time point, no common TBI-gene alterations were identified across the two genotypes analyzed (**Fig. 3A**).

Pathway enrichment analysis on the significant TBI-dysregulated genes from GFAP^{P301L} astrocytes was not possible to perform due to the low number of DEGs. However, in the CamkIIα^{P301L} cohort, IPA analysis of the 579 DEGs revealed 191 significantly modulated pathways that include the upregulation of *phagosome formation, neuroinflammation, NO and ROS production, and leukocyte extravasation*; and the downregulation of *triacylglycerol biosynthesis, fatty acid oxidation, oxidative phosphorylation, and neurovascular coupling* (**Fig. 3D**) - see also **Fig 4**.

⇒ *Collectively, these enriched pathways suggest that at 6 months post-injury CamkIIα^{P301L}-derived astrocytes exhibit a progressive and persistent injury associated phenotype with a diminished bioenergetic activity, proinflammatory state and oxidative stress compared to WT and GFAP^{P301L} astrocytes.*

Major Task 3 (Sub task – 3a)

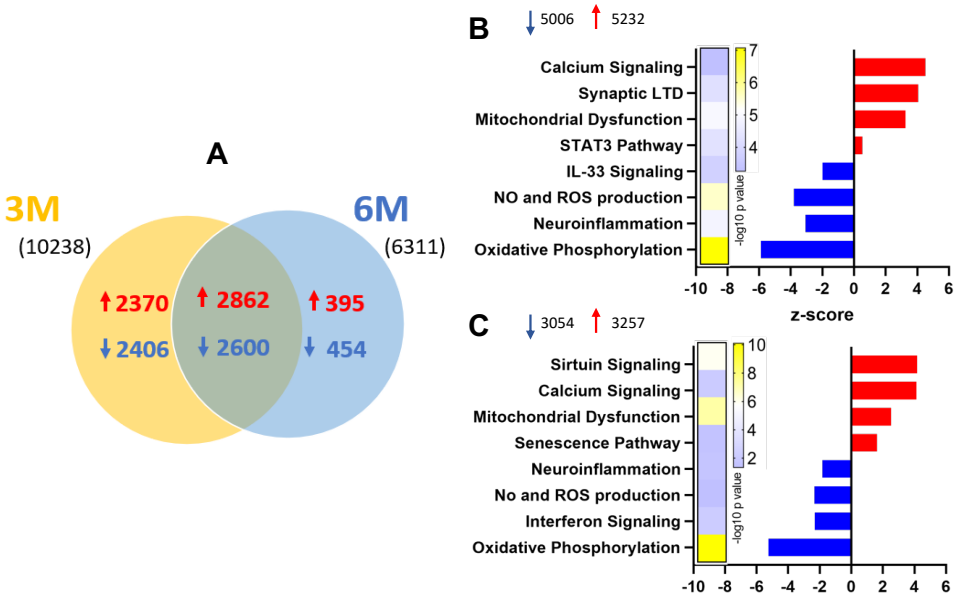

Figure 5. Astrocytic dysregulated pathways in aged GFAP^{P301L} 16- and 19-month-old mice compared to Wild-type. Venn diagram of DEG's (A). Upregulated (red) and downregulated (blue) pathways in GFAP-P301L vs WT astrocytes at 16 mos (B) and 19 mos (C) post-last injury. Threshold for obtaining the DEGs: adj. p-value≥0.05 with its respective –log value≥1.3. N=6 mice/group (N=3 technical replicates)

SUMMARY

GFAP^{P301L} and WT mice were subjected to our 20-hit model of r-mTBI at the age of **12 months** (aged cohort). Astrocytes from TBI and Sham mice were magnetically isolated using ACSA2+ antibody beads at 3 and 6 months post-last injury. RNA was isolated and sent to Azenta for next generation sequencing.

Firstly, we performed bioinformatic analysis of astrocyte transcriptome in sham mice between the aged GFAP-P301L vs WT model at 16 mo (3 mo timepoint) and 19 mo of age (6 mo timepoint) to delineate any genotype specific effects in the pathogenic tau bearing astrocyte model. We revealed that GFAP^{P301L} astrocytes at 16mo, showed 10,238 DEG's compared to their WT counterparts. While at 19mo, GFAP^{P301L} astrocytes revealed 6311 DEG's compared to their WT counterparts (**Fig 5A**). Gene ontology reveled that at both timepoints, astrocytes exhibited an increase in pathways relating to mitochondrial dysfunction and calcium signaling in GFAP-P301L vs WT mice (**Fig 5A-B**). Intriguingly, astrocytes from the GFAP^{P301L} model also showed an **immunosuppressed phenotype** compared to WT astrocytes at both timepoints (**Fig 5A-B**).

This suggests that pathogenic/P301l-mutant human tau upregulation in astrocytes impairs mitochondrial function and bioenergetics, results in aberrant calcium signaling, and contributes to an immunosuppressed astrocyte phenotype.

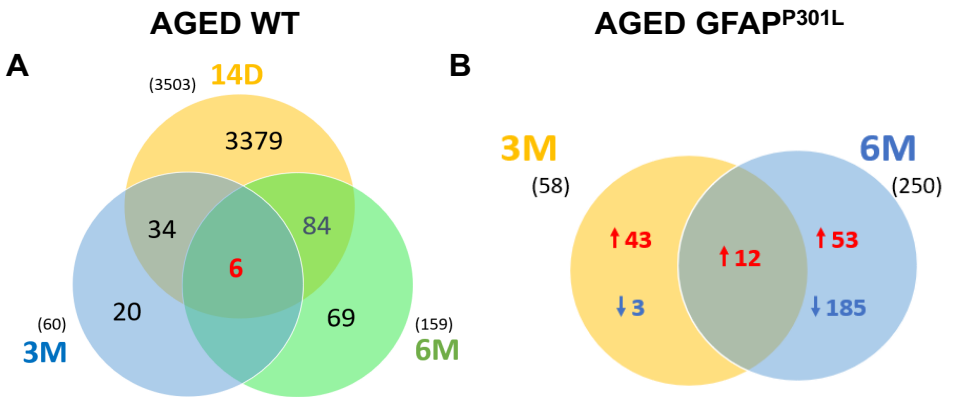

Figure 6. Differentially expressed genes (DEG's) in ACSA2+ astrocytes isolated from aged WT and GFAP^{P301L} r-mTBI vs sham mice. Venn diagram showing the overlap of TBI-dependent astrocytic DEGs (r-mTBI vs sham) across the different timepoints post-injury in WT (A) and GFAP^{P301L} mice (B). Threshold for obtaining the DEGs: adj. p-value≥0.05 with its respective –log value≥1.3. N=6 mice/group (N=3 technical replicates)

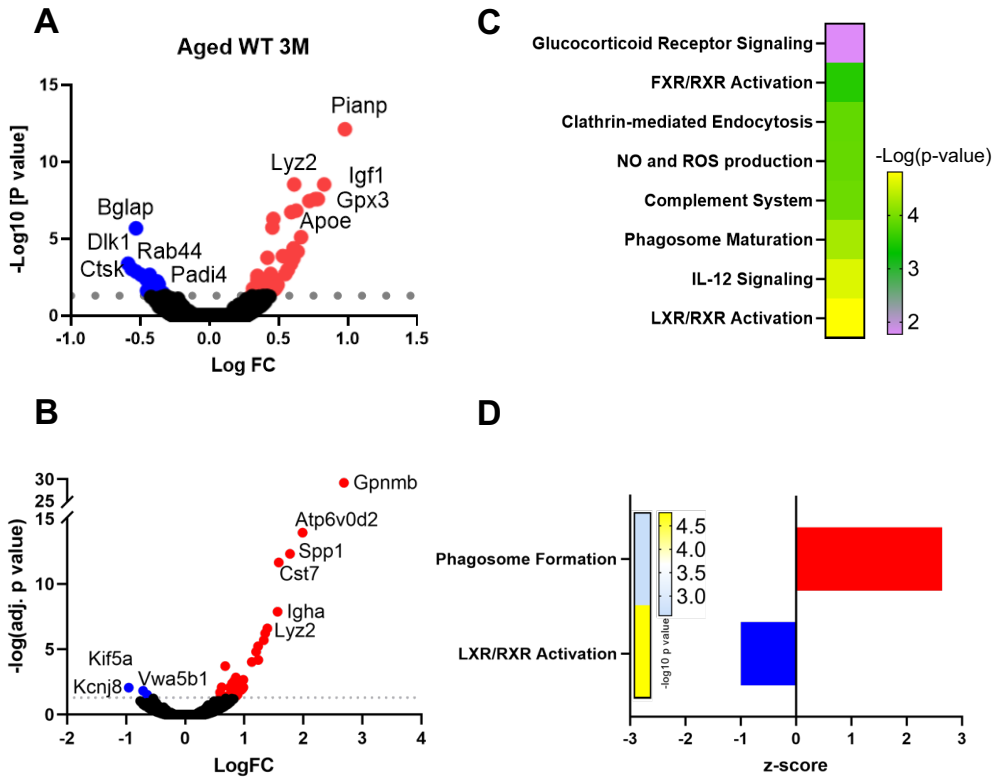

Figure 7. Differentially expressed genes (DEG's) and dysregulated pathways in ACSA2+ astrocytes isolated from Aged WT and GFAP^{P301L} r-mTBI vs sham mice at 3 months post-injury. Volcano plot of DEGs in WT (A) and GFAP^{P301L} (B) r-mTBI vs sham astrocytes at 3 months post-last injury. Upregulated and downregulated pathways in WT (C) and GFAP^{P301L} (D) r-mTBI vs sham astrocytes at 3 months post-last injury. Threshold for obtaining the DEGs: adj. p-value≥0.05 with its respective –log value≥1.3. N=6 mice/group (N=3 technical replicates)

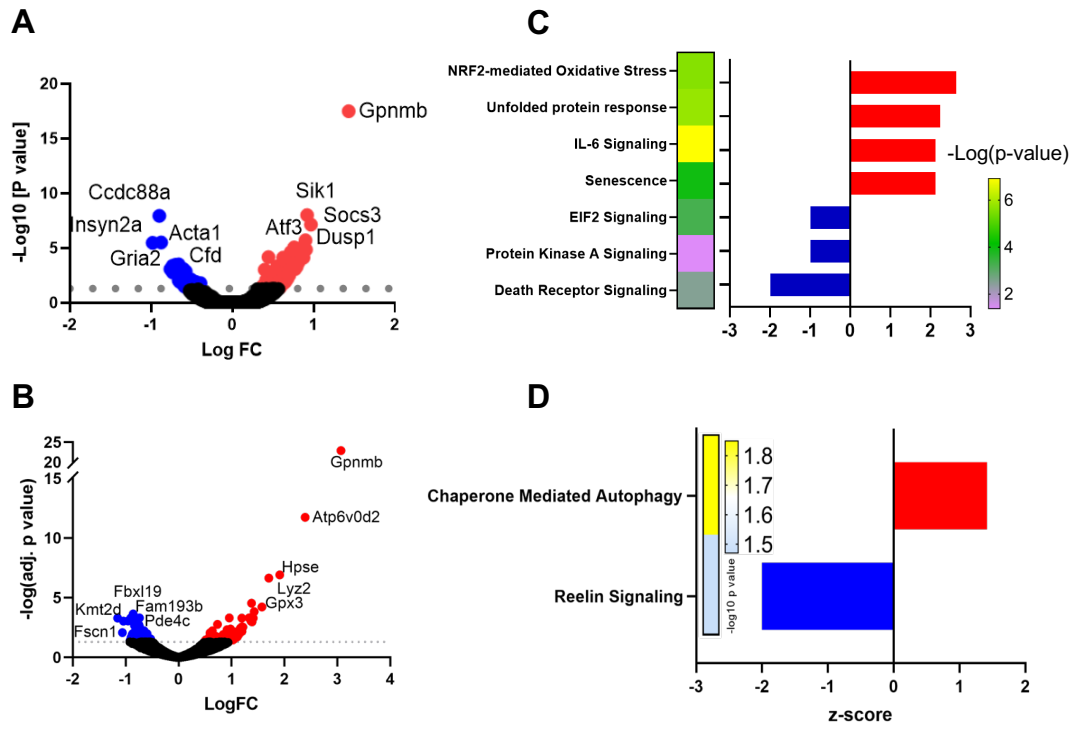

Figure 8. Differentially expressed genes (DEG's) and dysregulated pathways in ACSA2+ astrocytes isolated from Aged WT and GFAP^{P301L} r-mTBI vs sham mice at 6 months post-injury. Volcano plot of DEGs in WT (A) and GFAP^{P301L} (B) r-mTBI vs sham astrocytes at 6 months post-last injury. Upregulated and downregulated pathways in WT (C) and GFAP^{P301L} (D) r-mTBI vs sham astrocytes at 6 months post-last injury. Threshold for obtaining the DEGs: adj. p-value≥0.05 with its respective –log value≥1.3. N=6 mice/group (N=3 technical replicates)

Summary

Aged WT cohort

In Aged WT mice, we observed the greatest astrocyte transcriptomic response at 14 days post-injury (**Fig. 6A**), but this effect was diminished by 3- and 6-months post-injury (**Fig 6A, 7A, 8A**). In comparison with our young cohort, we observed 57 DEG's at 3 months post-injury, suggests comparable effects at this timepoint in young vs aged WT cohorts. Because we are missing data from the 6-month young WT cohort, we are unable to make comparisons at this timepoint.

At 3 months (**Fig 7C**), pathway analyses of the aged cohort revealed alterations in glucocorticoid, NO/ROS production, RXR and complement pathway and phagosome formation. Likewise in the young cohort - complement pathway and phagosome formation were also altered (**see Fig 2**). But differences were also observed such as insulin, CREB, GPCR and phospholipase C signaling in young mice and clathrin mediated endocytosis, IL12, glucocorticoid receptor and LXR/RXR signaling in Aged WT mice at 3 months.

At 6 months, Injured Aged astrocytes exhibited an increase in NFR2 mediated oxidative stress, UPR, IL8 and cell senescence signaling, and a downregulation in ERF2 and PKA signaling (**Fig 8C**). Top upstream regulators in Aged injured astrocytes were PDGF, CREB1, IL1B and GPER1 (**not shown**).

Aged GFAP^{P301L} cohort

In the TBI vs sham comparisons, bioinformatic analysis revealed that at 3mo post-last injury, astrocytes from aged GFAP^{P301L} r-mTBI brains had 58 differentially expressed genes (DEGs) compared to sham brains. The number of DEG's was ~4x higher when mice were allowed to age for 3 more months (6mo post last injury) **Fig. 6B, 7B, 8B**. In comparison with the young cohort – we observed more genes at the 3-month timepoint (441 vs 58), but less at the 6-month timepoint compared to the aged cohort (5 vs 250), signifying the ageing may have a more detrimental progressive and chronic lasting effect on TBI response by astrocytes in GFAP^{P301L} mice (**see Fig 2A and 3A**).

IPA analysis of the DEG's at the 3mo post last injury timepoint revealed upregulation of phagosome formation. Additionally, pathways involved in regulation of lipid metabolism was downregulated (**Fig. 7D**). Compared to the young GFAP^{P301L} cohort, we observed a different transcriptomic profile typified by upregulation of complement systems, neuroinflammatory signaling, PKA and ERK5 signaling, and downregulation in oxidative phosphorylation, mTOR signaling and synaptic LTP related pathways (**Fig 2F**).

At the 6mo post-last injury timepoint in the aged GFAP^{P301L} cohort, autophagy signaling pathway was upregulated and the reelin signaling pathway was downregulated. The latter is involved in neuronal growth, maturation, and synaptic activity (**Fig. 8D**). Only 5 genes were altered in the young cohort therefore no pathways were identified by IPA analyses.

These datasets thus suggests that TBI influences aged tau bearing astrocytes negatively by diminishing their lipid metabolic processes and neuronal supportive mechanisms.

Analysis of the Top upstream regulator (UPR) driving these transcriptomic changes in GFAP-P301L TBI vs sham astrocytes, included inhibition of NPC1 and activation of SNCA, CSF1, TGFBR2 and PLCG2 (**not shown**), at both 3 and 6 months post-last injury. Several of these activated UPR genes are involved in the regulation of inflammatory processes and may thus indicate a TBI mediated effect on inflammatory signaling pathways.

Aim 2 - Part two: Single cell genomic profiling of astrocyte populations in autopsied brains from TBI cases.

Major Task 3 (Sub task – 1)

Given the minimal effects observed in astroglial markers from our TBI autopsy vs control cases, in our LCM study, we decided to use TBI cases with CTE neuropathological change and notable tauopathy. All analyses were conducted in the hippocampus as this was the brain region available for these studies.

GENE ARRAY ANALYSES OF MICRODISSECTED ASTROGLIA IN AUTOPSY TBI TISSUE

Table 1 shows group classification and history of de-identified patients analyzed for astroglia gene array. Sample sizes range from 10-12.

Table 1: Group Classification and History

	CTE II	CTE III	CTE IV	p-value	Groupwise Comparison
Age at Death	54.92±22.03	65.36±11.08	77.36±8.26	0.01	IV > II
Age Began Playing	12.00±3.36	12.73±1.95	11.36±2.25	0.37	na
Years Played	14.00±5.08	16.27±5.08	16.64±6.25	0.48	na
Years Between Retirement and Death	28.92±20.78	36.36±11.21	49.36±11.41	0.03	IV > II
Age at Symptom Onset	43.18±21.29	44.73±18.61	59.91±14.58	0.07	na

	group					
	cte_2		cte_3		cte_4	
	Mean	SD	Mean	SD	Mean	SD
age	54.917	22.0349	65.364	11.0840	77.364	8.2616
age_begun	12.000	3.3575	12.727	1.9540	11.364	2.2482
age_symonset	43.182	21.2923	44.727	18.6069	59.909	14.5839
calc_yrsrettodeath	28.917	20.7779	36.364	11.2096	49.364	11.4129
yrs_play	14.000	5.0812	16.273	5.0812	16.636	6.2494

METHODOLOGY

LASER CAPTURE MICRODISSECTION (LCM)AND GENE TRANSCRIPT PROFILING:

A laser capture microdissection (LCM) instrument (Mufson lab) was used for these studies. LCM methodology results in accurate dissection of the astroglial cells of interest with minimal disruption of the surrounding tissue. For the proposed studies, GFAP-positive astroglia are captured per reaction, per condition for subsequent linear terminal continuation (TC) RNA amplification and microarray analysis. TC RNA amplification was developed in Dr. Ginsberg's laboratory. The method entails synthesizing first strand cDNA complementary to the RNA template, generating second strand cDNA complementary to the first strand cDNA, and finally *in vitro* transcription using the double stranded cDNA as template. This process displays high fidelity, reproducibility and increased signal sensitivity (4-fold) and flexibility compared to other RNA amplification protocols. Radiolabeled RNA probes will be hybridized to custom-designed microarrays. Array platforms consist of 1µg of linearized cDNA purified from plasmid preparations adhered to high-density nitrocellulose (Hybond XL, GE Healthcare, Piscataway, NJ) using an arrayer robot (VersArray, Bio-Rad, Hercules, CA) (Ginsberg, 2005, 2008). Each cDNA and/or expressed sequence-tagged cDNA (EST) was verified by sequence analysis and restriction digestion. Human clones are employed on the custom-designed array. Approximately 864

cDNAs/ESTs organized into 22gene ontology groups are present on the current array platform. Dr. Ginsberg has already successfully and productively transferred this technology to Dr. Mufson's laboratory at Barrow Neurological Institute, which is where these experiments were carried out.

Statistical procedures (using GeneLinker Gold**)** for custom-designed microarray analysis have been described in detail previously (Ginsberg et al., 2014; 2016; 2017; Mufson et al., 2017). Gene expression differences will be assessed with respect to the hybridization signal intensity ratio of the total signal of all array genes. For each gene the signal intensity ratio is modelled as a function of study group, using mixed effects models with random effect to account for the correlation between repeated assays. Between subject versus within-subject variation will be analyzed by random intercept, fixed effect covariate, Kenward-Roger denominator degrees of freedom, unstructured covariance structure, and log-transformed expression levels. Significance will be judged at the level α=0.01, two-sided; false discovery rate (FDR) based on an empirical null distribution due to strong correlation between genes is controlled at level α=0.1. Spearman's coefficient will evaluate correlations of select transcripts. Serial section *in situ* hybridization will confirm changes in transcript expression.

Preliminary findings presented below from staged TBI groups vs controls – Major Task 3 (Subtask 1)

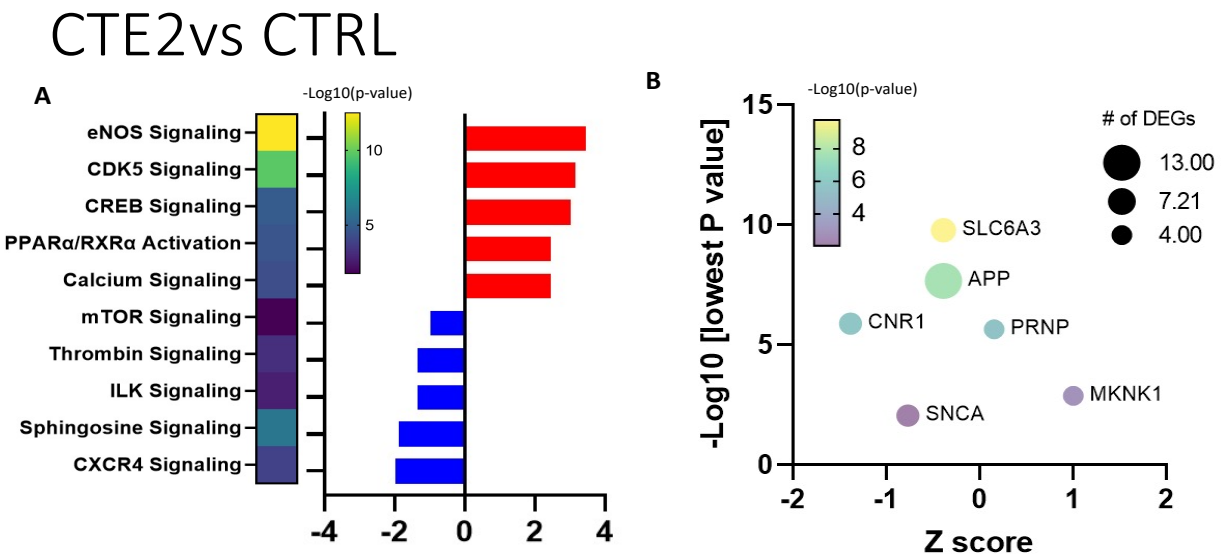

Figure 1. Pathway and Upstream regulator analysis on cases of CTE (stage 2). A) Top 5 upregulated pathways in red and top 5 downregulated pathways in blue. B) Bubble plot of the top 6 upstream regulators. DEGs=differentially expressed genes.

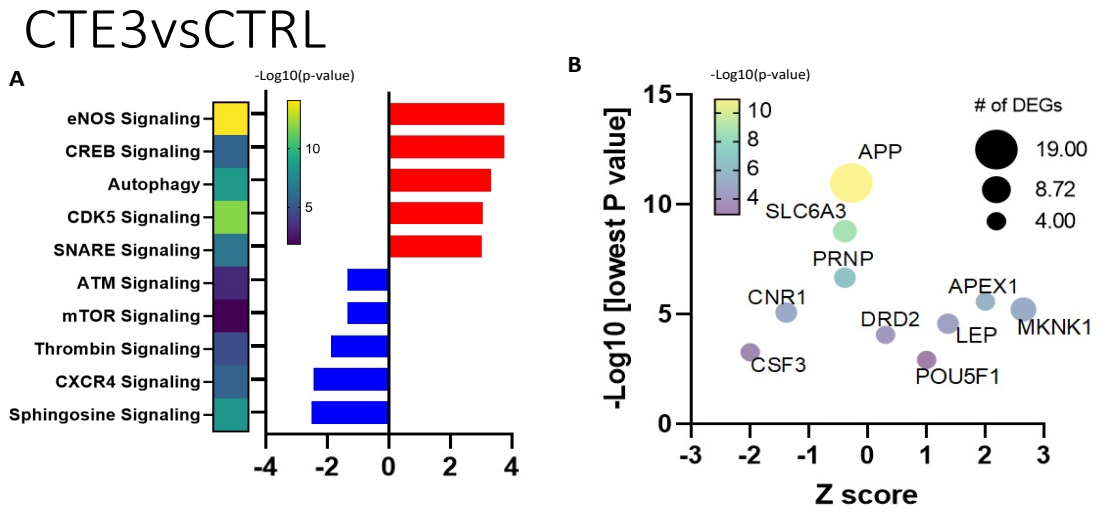

Figure 2. Pathway and Upstream regulator analysis on cases of CTE (stage 3). A) Top 5 upregulated pathways in red and top 5 downregulated pathways in blue. B) Bubble plot of the top 10 upstream regulators. DEGs=differentially expressed genes.

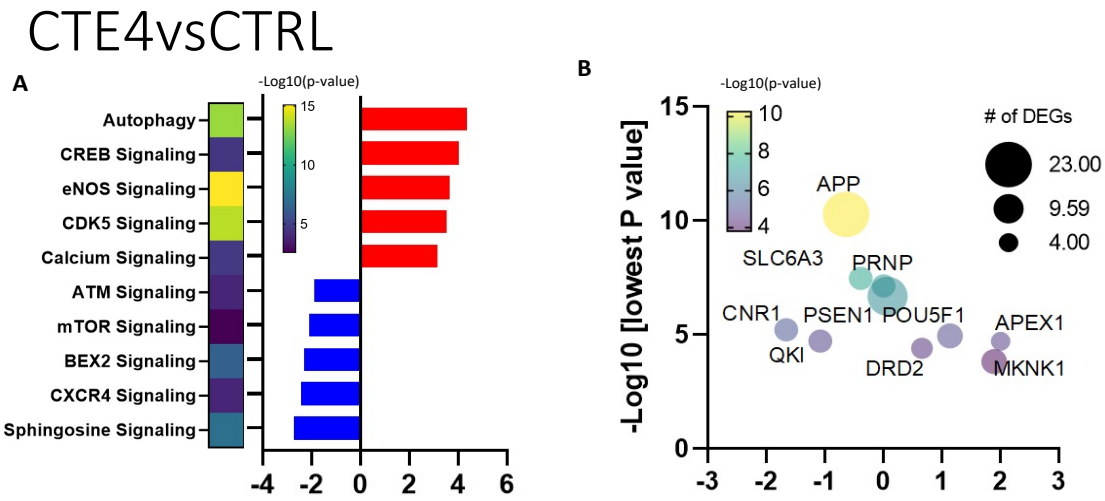

Figure 3. Pathway and Upstream regulator analysis on cases of CTE (stage 4). A) Top 5 upregulated pathways in red and top 5 downregulated pathways in blue. B) Bubble plot of the top 10 upstream regulators. DEGs=differentially expressed genes.

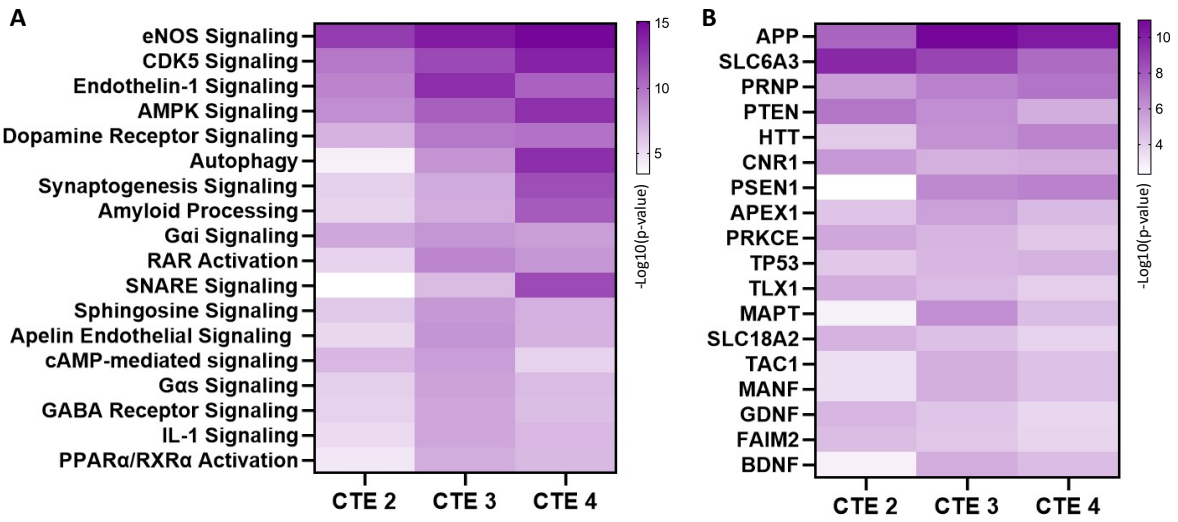

Figure 4. Comparative pathway and upstream regulator analysis among CTE stages (2-4): A) comparative analysis on the top 20 altered pathways B) comparative analysis on the top 20 upstream regulators

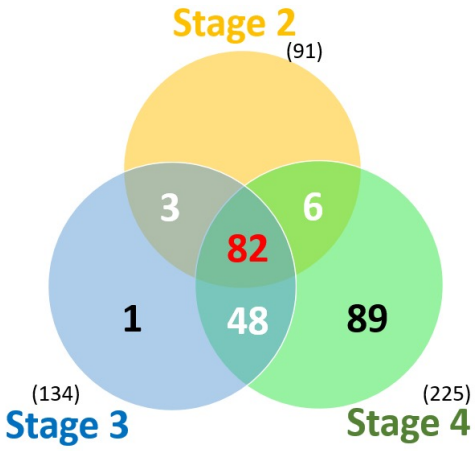

Figure 5. Venn-diagram of differentially expressed genes in astrocytes from CTE brains at the various stages (2-4).

Ontology	Gene	P-value	Groupwise Comparison
AD related genes	ARMCX2	0.0005	CTE-2<CTE-4
	B2M	0.0002	CTE-2<CTE-4
	BACE2	0.0004	CTE-2<CTE-4
	PRNP	0.003	CTE-2<CTE-4
	PSEN2	0.0002	CTE-2<CTE-4
	SAA4	0.003	CTE-2<CTE-4
	MAPT6	0.03	CTE-2<CTE-4
	MAPT5	0.02	CTE-2<CTE-4
Ionic channels	DPP10	0.003	CTE-2<CTE-4
Cytoskeletal elements	CDH2	0.001	CTE-2<CTE-4
	LAMB2	0.002	CTE-2<CTE-4
Cell death related genes	AIFM1_PCD8	0.0008	CTE-2<CTE-4
	CCNG1	0.03	CTE-2<CTE-4
	CCNF	0.02	CTE-2<CTE-4
	CCNB1	0.02	CTE-2<CTE-4
	CASP9	0.009	CTE-2<CTE-4
	CASP5	0.04	CTE-2<CTE-4
	CASP4	0.03	CTE-2<CTE-4

Table 1. Groupwise analysis among human cases of CTE at the different stages (2-4).

Summary of findings (human autopsy LCM/gene array)

1) We observed a significant upregulation in autophagy, cdk5, CREB, calcium and eNOS signaling in CTE stages vs controls. These effects were more prominent in CTE4 vs control cases. See **Figure 1-3 and Figure 4A.**
2) We observed a significant downregulation in mTOR, CXCR4, sphingosine pathways in all CTE stages vs controls. See **Figure 1-3** and **Figure 4A**.
3) Top upstream regulator in CTE2 vs Control cases was SLC6A3 (**Figure 4B**). Top upstream regulator in CTE3 vs control and CTE4 vs control was APP.
4) Venn diagram in Figure 5 shows 88 and 130 genes shared between 'CTE2 vs control & CTE4 vs control' and 'CTE3 vs control & CTE4 vs control' comparisons, respectively. Notable CTE4 vs control comparison also revealed a large number of unique significantly regulated genes (89) not shared between comparisons of CTE2 vs control and CTE3 vs control. **See Figure 5**
5) Groupwise analyses revealed a significant positive correlation in ADRD genes, genes related to cell death and cytoskeletal element with TBI staging.

Thus, these data reveal that CTE astrocytes are compromised and exhibit loss of neurorestorative function(s) and in the most severe CTE stage (CTE-IV) such changes are prominently accompanied by an immunosuppressed state compared to controls.

Additionally, we looked for similarities in enriched pathways between the CTE-IV astrocytes and astrocytes from our mouse models. Firstly, CTE-IV astrocytes show slightly more similarities with astrocytes harvested from the sham GFAP^{P301L} vs WT astrocytes than CamkIIα^{P301L} vs WT astrocytes, with 20 and 12 identified pathways in common, respectively. Similarities with sham GFAP^{P301L} astrocytes include the significant immunosuppressed response characterized by the downregulation of *IL-8 signaling and NO and ROS production*. Similarities with sham CamkIIα^{P301L} astrocytes include decreased *neurovascular coupling signaling*. On the other hand, CTE-IV astrocytes revealed three times more pathways in common with GFAP^{P301L} r-mTBI vs sham astrocytes than CamkIIα^{P301L} r-mTBI vs sham astrocytes at 3 months post-last injury. CTE-IV - GFAP^{P301L} similarities include the downregulation in *synaptogenesis* and *calcium signaling*. CTE-IV - CamkIIα ^{P301L} similarities include downregulation of *erythropoietin signaling*.

What opportunities for training and professional development has the project provided?
If the project was not intended to provide training and professional development opportunities or there is nothing significant to report during this reporting period, state "Nothing to Report."

Describe opportunities for training and professional development provided to anyone who worked on the project or anyone who was involved in the activities supported by the project. "Training" activities are those in which individuals with advanced professional skills and experience assist others in attaining greater proficiency. Training activities may include, for example, courses or one-on-one work with a mentor. "Professional development" activities result in increased knowledge or skill in one's area of expertise and may include workshops, conferences, seminars, study groups, and individual study. Include participation in conferences, workshops, and seminars not listed under major activities.

Nothing to Report

How were the results disseminated to communities of interest?
If there is nothing significant to report during this reporting period, state "Nothing to Report."

Describe how the results were disseminated to communities of interest. Include any outreach activities that were undertaken to reach members of communities who are not usually aware of these project activities, for the purpose of enhancing public understanding and increasing interest in learning and careers in science, technology, and the humanities.

Nothing to Report

What do you plan to do during the next reporting period to accomplish the goals?
If this is the final report, state "Nothing to Report."

Describe briefly what you plan to do during the next reporting period to accomplish the goals and objectives.

NOTHING TO REPORT (N/A)

4. **IMPACT:**

What was the impact on the development of the principal discipline(s) of the project?

Nothing to Report

What was the impact on other disciplines?

Nothing to Report

What was the impact on technology transfer?

Nothing to Report

What was the impact on society beyond science and technology?

Nothing to Report

5. CHANGES/PROBLEMS:

Changes in approach and reasons for change

Nothing to Report

Actual or anticipated problems or delays and actions or plans to resolve them

Nothing to Report

Changes that had a significant impact on expenditures

Nothing to report

Significant changes in use or care of human subjects, vertebrate animals, biohazards, and/or select agents

Significant changes in use or care of human subjects

N/A

Significant changes in use or care of vertebrate animals

Nothing to report

Significant changes in use of biohazards and/or select agents

Nothing to report

6. PRODUCTS:

- **Publications, conference papers, and presentations**

Journal publications.

Nothing to report (In progress, two manuscripts planned for submission in June 2024)

Books or other non-periodical, one-time publications.

Nothing to report

Other publications, conference papers and presentations.

Posters –

Neurotrauma meeting 2021 - online symposium: Camila Ortiz, Andrew pearson, Benoit Mouzon, McKenzie Browning, Robyn McCartan, Michael Mullan, Elliott Mufson, Fiona Crawford, Joseph Ojo. Temporal changes in astrocyte gene profiles in the aftermath of repetitive mild traumatic brain injury in human tau mouse models.*

Neurotrauma meeting 2022 - Atlanta symposium: Camila Ortiz, Andrew pearson, Benoit Mouzon, McKenzie Browning, Robyn McCartan, Michael Mullan, Elliott Mufson, Fiona Crawford, Joseph Ojo. Tau astrogliopathy in the aftermath of repetitive mild traumatic brain injury in human tau mouse models.*

Neurotrauma meeting 2023 - Austin symposium: Camila Ortiz, Andrew pearson, Benoit Mouzon, McKenzie Browning, Robyn McCartan, Michael Mullan, Elliott Mufson, Fiona Crawford, Joseph Ojo. Overexpression of pathogenic human tau in astrocytes induces transcriptomic changes following to r-mTBI leading to cellular dysfunction.*

- **Website(s) or other Internet site(s)**

Nothing to report (roskampinstitute.org website will highlight the results of our findings once our two manuscripts planned for middle of 2024 have been accepted for publication).

- **Technologies or techniques**

Nothing to report

- **Inventions, patent applications, and/or licenses**

Nothing to report

- **Other Products**

Nothing to report

7. PARTICIPANTS & OTHER COLLABORATING ORGANIZATIONS

What individuals have worked on the project?

Name: *Fiona Crawford (no change)*
Project Role: *PI*
Researcher Identifier (e.g. ORCID ID): *N/A*
Nearest person month worked: *1.2*
Contribution to Project: *Dr Crawford directs all aspects of this project and provides supervision on the overall approach and data interpretation for the experiments outlined in this application. In particular, she will interact with all of the team members listed on this application and provide full oversight as they implement the work proposed in this application, including regular communication with the expert consultants.*

Name: *Joseph Ojo (no change)*
Project Role: *Co-PI*
Researcher Identifier (e.g. ORCID ID): *N/A*
Nearest person month worked: *2.4*
Contribution to Project: *Dr. Ojo works alongside Dr. Crawford in directing all aspects of this project and providing supervision on mTBI animal modeling, histopathological analyses and data interpretation. He is responsible for overseeing all aspects of animal manipulation and ensuring that the projects are executed in a timely fashion. He will also perform histopathological assessments in both humans and animal models as described in the proposal.*

Name: *Camila Ortiz (no change)*
Project Role: *Graduate Student*
Researcher Identifier (e.g. ORCID ID): *N/A*
Nearest person month worked: *12*
Contribution to Project: *Camila Ortiz was involved in animal handling and surgical procedures, as well as histopathological characterization and molecular and in vitro analyses. She assisted in all surgical procedures (primarily years 1 and 2) and conducted histopathological analyses with the supervision of Dr. Ojo (primarily Years 2 & 3). She also performed bioinformatic studies in Years 3 and 4.*

Has there been a change in the active other support of the PD/PI(s) or senior/key personnel since the last reporting period?

Nothing to Report

What other organizations were involved as partners?
)

Nothing to Report

8. **SPECIAL REPORTING REQUIREMENTS**
   COLLABORATIVE AWARDS: *N/A*
9. **QUAD CHARTS:** *N/A*
10. **APPENDICES:** *N/A*

Astroglia Pathobiology in the Neurodegenerative Sequelae of Repetitive Mild TBI

Log number AZ180123

W81XWH-19-1-0535

PI's: Drs Fiona Crawford & Joseph Ojo **Org:** Roskamp Institute, Sarasota, FL **Award Amount:** $718,000

Study Aim 1: Delineation of the effects of chronic repetitive mTBI on astrocyte pathobiology and related proteinopathy in tau bearing preclinical models at multiple time points post-injury, and validation in autopsied brains from human TBI/ADRD cases. **Study Aim 2:** Evaluating pathobiological effects of reactive/injured astrocytes derived from TBI models, on the induction and spreading of age-related proteinopathies and neurodegeneration. **Study Aim 3:** Generation of single cell omic profiles in different populations of astrocytes obtained from preclinical models and validation in autopsied brains from human TBI/ADRD cases.

Approach

i) Histopathological assessment of astrocyte pathobiology in WT, TauKI and GFAP-Tau^{WT} mouse models exposed to r-mTBI or sham injury, when young (3 mos) or aged (12mos) and analyzed at 3 and 6mos post-injury. Histopathological assessment of astrocyte lesions in human ADRD/TBI cases.

ii) Adoptive transfer of TBI astrocytes into naïve mice (in vivo), and exposure of TBI astrocyte secretomes to healthy neural/vascular cells (ex vivo). Assessment of pathobiological changes induced by reactive astrocytes.

iii) Single cell omic profiles of astrocytes obtained from models above. Validation of distinct astrocyte cell population of interest and gene profiles using flow cytometry and cell sorting. Single cell gene profiles of astrocytes from autopsied human brains.

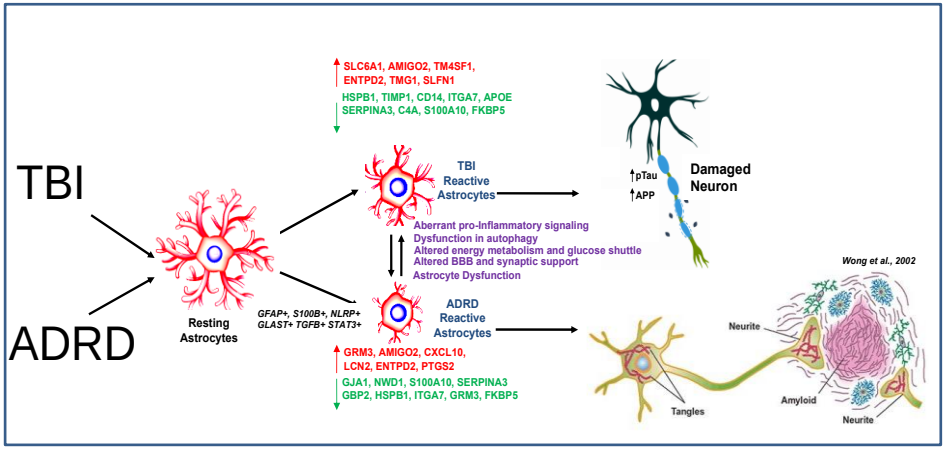

Accomplishment: (1) Histopathological and biochemical analyses of the hippocampus and cortex from tau Tg mouse models of r-mTBI at 3 & 6 mos post-injury. (2) Analyses of cytokine profiles in astrocyte secretomes from TBI vs sham mice. (3) Analysis of the effects of exposing quiescent microglial and naïve mice to secretome from TBI vs sham astrocytes. (4) RNAseq of astrocytes from TBI vs sham mouse models, and correlation with human autopsy cases.

Timeline and Cost

Activities CY	19-20	20-21	21-23
MAJOR TASK ONE OR AIM 1			
MAJOR TASK TWO OR AIM 2			
MAJOR TASK TWO OR AIM 3			
Estimated Direct Budget (500K)	**$129K**	**$205K**	**$166K**

Last updated: (September 2022)

Goals/Milestones

CY19 Goal

☑ Obtain regulatory approval to begin animal and human specimen studies

CY20 Goals

☑ Breeding and administering injuries to different mouse models

☑ Begin histological assessment of human control/TBI/ADRD brains tissue

☑ Begin gene analyses of microdissected astrocyte from autopsy brain tissue

CY21 Goals

☑ Histological assessment of astrocyte and proteinopathy in mouse models

☑ Conduct adoptive transfer studies and ex vivo functional assay studies.

☑ Complete human histological and gene array analyses

CY22-23 Goal

☑ Gene/protein analyses of astrocyte from mouse models

☑ Validation experiments of gene array/proteomic findings in mice/humans

Comments/Challenges/Issues/Concerns

- Imaging for mouse histopathology staining impacted by COVID restrictions.
- LCM needed replacement, and LCM work was held back by a few months.

Projected Expenditure: $718,349 **Actual Expenditure**: $718,349